ISSN 0016-8521, Geotectonics, 2017, Vol. 51, No. 3, pp. 209–229. © Pleiades Publishing, Inc., 2017.
Original Russian Text © E.P. Dubinin, Yu.I. Galushkin, A.L. Grokholskii, A.V. Kokhan, N.M. Sushchevskaya, 2017, published in Geotektonika, 2017, No. 3, pp. 3–27.

Hot and Cold Zones of the Southeast Indian Ridge and Their Influence on the Peculiarities of Its Structure and Magmatism (Numerical and Physical Modelling)

E. P. Dubinin[a], *, Yu. I. Galushkin[a], A. L. Grokholskii[a], A. V. Kokhan[b], and N. M. Sushchevskaya[c]

[a] *Moscow State University, Moscow, 119991, Russia*
[b] *Svarog LLC., Moscow, 119021, Russia*
[c] *Institute of Geochemistry and Analytical Chemistry, Russian Academy of Sciences, Moscow, 119991, Russia*
**e-mail: edubinin08@rambler.ru*

Received November 22, 2016

Abstract—The paper describes the specific features of the bottom topography and morphostructural segmentation along the strike of the Southeast Indian Ridge (SEIR) and in the zones of influence of the Amsterdam–St. Paul hot spot and the anomalous zone of the relatively cold mantle in the area of the Australian–Antarctic discordance. Numerical estimates of changes of thermal state and strength of the crust in axial and off-axial zones of the SEIR were performed. Correlation between the thermal–rheological settings in the axial zone of the ridge with the seabed topography and the morphostructural segmentation and magmatism has been established. The numerical modelling results make it possible to assume the presence of along-axis asthenospheric flows under the axial zone of the SEIR. One of them, which was initiated by the Amsterdam–St. Paul point and the Kerguelen plume, is oriented from west to east, and the second, located east of the Australian–Antarctic discordance, is oriented from east to west. Taking into account the numerical modelling results of the thermal regime and the change in thickness of the brittle layer of the axial lithosphere, we performed a physical modelling of the influence of temperature anomalies in the mantle on the peculiarities of crustal deformation in the axial zones of the ridge. The experimental modelling showed that the presence of a thermal anomaly in the sublithosphere mantle in the form of a local heat source (hot spot) will noticeably influence the geometry of the rift axis and its position in relation to the hot spot. An area of anomalous topography forms under the influence of the hot spot, traces of which are preserved in the off-axis spreading flank zones, as in the case of the Amsterdam–St. Paul hot spot. More contrasting and dissected topography forms in zones with a relatively low typical mantle temperature in the process of crustal accretion.

Keywords: Southeast Indian Ridge, topography, segmentation, numerical and physical modelling, thermal anomalies in mantle, magmatism, accretion, ridge structures

DOI: 10.1134/S0016852117030049

INTRODUCTION

The study of the peculiarities of the change in morphology, anomalous potential fields, and the deep structure of spreading ridges associated with mantle temperature variations in the areas of occurrence of hot spots and mantle plumes attracted attention of researchers [1, 4–6, 16, 18, 20, 27, 46]. The nature of interaction of a hot spot and a spreading ridge is determined by the duration of its functioning, the mantle temperature, the spreading rate, and the distance between them. These factors determine the features of crustal accretion, the intensity of magma supply, the nature of the occurrence of recent volcanism, the anomalous structure of the topography of axial and off-axial spreading zones, increased thickness of the crust, and many other indicators.

Another important study is that of the influence of zones with a relatively cold sublithosphere mantle on the morphology of spreading ridges. Nowadays such examples can be observed in the region of the equatorial Atlantic with the system of the gigantic Romanche, Chain, and Charcot transform faults, which displace the spreading axis by hundreds of kilometers, the area of the Australian–Antarctic discordance at the Southeast Indian Ridge (SEIR), etc. All these areas are characterized by a rugged seabed topography and intense gravity anomalies.

The SEIR is a remarkable example where both anomalously heated zones associated with the presence of the Amsterdam–St. Paul (ASP) hot spot, located nearly on the spreading axis, and the Kerguelen plume, the recent volcanic occurrences of which are located a significant distance from the spreading ridge; as well,

anomalously cold zones of the lithosphere and the sublithospheric mantle—the Australian-Antarctic discordance (AAD)—are found along the ridge strike.

According to [46], the SEIR interacted with the ASP hot spot in three stages starting from a period of about 10–12 Ma ago. The ASP plateau started to form about 10 Ma ago owing to intensification of magmatism in neighboring segments. The SEIR was located in close proximity to the hot spot. At the second stage, which began 3–6 Ma ago, magmatic activity weakened. The spreading ridge crossed the hot spot about 3–4 Ma ago, when its activity was reduced. Starting from a period of 3 Ma ago, the activity of the hot spot restored, which led to the formation of the current ridge segmentation in this area. Pulses of the hot spot's magmatic activity led to fixation of ancient rift valleys and axial rises in the topography at the stages of its decreased and increased activity, these topographic forms were established north of the plateau, according to detailed studies.

The influence of the Kerguelen plume on the SEIR continued from the moment of separation of the Kerguelen plateau and the Broken plateau by the forming SEIR. The age of the most ancient magnetic anomalies in the section of the western part of the plateau has been determined as 33–34 Ma [61]. The Kerguelen plume influences the deep mantle of this area at a distance of about 1000 km [43, 55]. According to [56], the hot spot can influence the ridge while being located at a distance of 1000–1500 km away. The migration of the hot spot material towards the spreading ridge may occur along the channel or along the base of the lithosphere, the level of which increases towards the spreading axis [55].

The influence of the Kerguelen plume evidently changes the morphology of the SEIR rift zone at the section from the ASP to the AAD. It is assumed that in the area of the SEIR east of the ASP plateau, along-axis flow of the asthenosphere occurs, which is mostly formed by the Kerguelen plume and the ASP hot spot to a lesser extent. This flow moves east towards the AAD, under which there is an area with a relatively cold mantle [44]. The existence of the along-axis asthenosphere flow may govern the reduction of the mantle temperature in this area from west to east.

The aim of this work is to study by the means of numerical and physical modelling the peculiarities of the lithosphere thermal regime and structure-forming processes in areas of the SEIR rift zone influenced by temperature anomalies of the sublithosphere mantle.

TOPOGRAPHY, SEGMENTATION, AND SPECIFIC FEATURES OF MAGMATISM OF THE RIFT ZONE OF THE SOUTHEAST INDIAN RIDGE FROM 78° TO 130° E

The SEIR stretches in sublatitudinal direction from the Rodrigues Triple Junction (TJ) to the Macquarie TJ at approximately 8000 km (Fig. 1). This paper describes the segment from the ASP plateau (75°–78° E) to the AAD (120°–130° E), located between areas with a relatively hot (Kerguelen, ASP hot spot) and relatively cold (AAD) mantle. At this section of the ridge spreading with practically constant velocities of 6.5–7 cm/yr [22], a significant change in the ridge structure occurs from the area with the relatively more heated lithosphere near the ASP plateau towards the area with the relatively less heated lithosphere near the AAD (Figs. 2, 3a).

The topography of the rift zones of mid-ocean ridges (MORs) with a low opening rate (less than 4 cm/yr) was commonly formed by deep rift valleys about 30 km wide and about 1.5–3 km deep [44]. Axial rise with a width of approximately 30 km and height of approximately 400–500 m is typical of MOR rift zones with fast spreading (more than 8 cm/yr), such as the East Pacific Rise [42]. At intermediate spreading ridges, where the spreading rate varies from 4 to 8 cm/yr, the morphology of rifting zones is more variable. The Galapagos spreading center, the Juan de Fuca Ridge, the Chile Rise, the Pacific–Antarctic Ridge, and the SEIR are examples of these. Typical of these ridges are the morphology of the intermediate type and along-axis changes in the morphology from rift valleys to axial rises through transit forms (Figs. 2, 3). Among the latter, reduced axial rises up to 10 km wide, dissected by grabens up to 100–200 m deep, and reduced rift valleys up to 10–15 km wide and up to 400–500 m deep are observed. The nature of the change in ridge structure is regular and coincides with the deep structure of the rift zone [24]. In some areas, the predominant macroform of the ridge topography is not traced and they are classified as areas with transit morphology.

During the study of the MOR rift zones, presence of axial magmatic chambers (AMC) was established by seismic methods on ridges with fast spreading [23] practically everywhere. The degree of saturation with the melt and roof shape of AMCs evidently determine the shape of the axial rise [44]. Stable AMCs are detected on the ridges with slow spreading with the up-to-date geophysical methods extremely rarely. Here, in the models of the deep structure of rift zones over the regional rise of the asthenosphere, the formation of individual centers of focused mantle upwelling is assumed, over which local short-living melt chambers can periodically occur in the crust [62]. Magma eruptions of the axial volcanoes at the bottom of the internal rift valley occur from these melt chambers. The presence or absence of a stationary AMCs in spreading ridges with high and low extension rates determines the fundamental differences in the accretion mechanisms, the deep structure of the crust, and the bottom topography of rift zones [2, 3, 29]. There is no such certainty in the models of the deep structure of the lithosphere for ridges with intermediate spreading rates today due to insufficiency of seismic surveys, although the topography of these ridges is described in

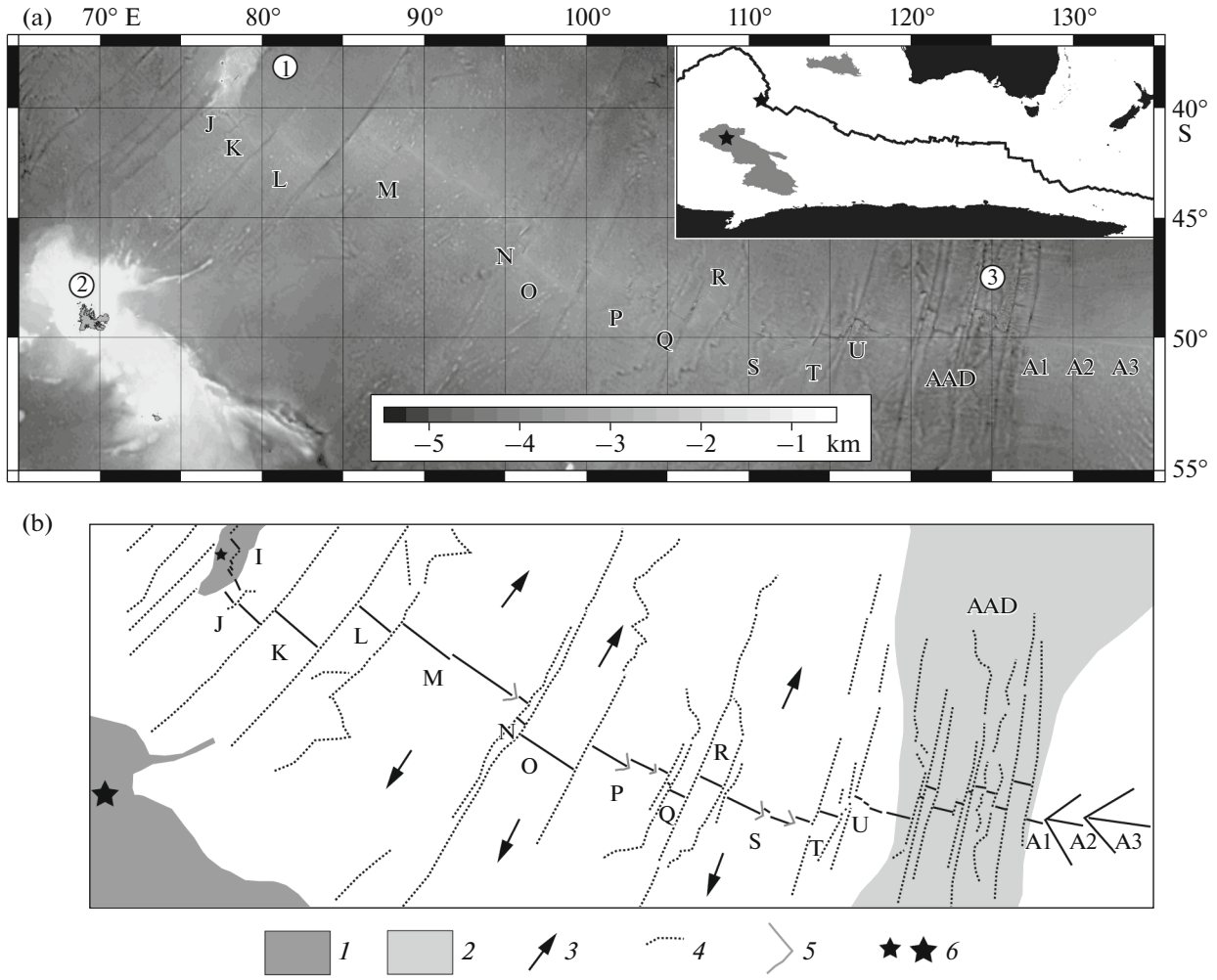

Fig. 1. Structure of SEIR in area from 78° to 135° E. (a) Bottom topography according to [31]. I–U, A1, A2, A3 is numeration of ridge segments according to [55, 58]. Numerals in circles indicate (1) Amsterdam–St. Paul plateau, (2) Kerguelen plateau, (3) Australian–Antarctic discordance. Position of SEIR in water area of southeastern part of Indian Ocean is shown in insert. (b) Ridge segmentation layout. I–U, A1, A2, A3 is numeration of ridge segments according to [55, 58]. (*1*) Amsterdam–St. Paul and Kerguelen plateau, (*2*) AAD zone, (*3*) spreading direction, (*4*) transform and nontransform faults of spreading axis and their off-axis traces, (*5*) propagating rifts and their off-axis traces, (*6*) center of Amsterdam–St. Paul hot spot and center of Kerguelen plume.

some detail (Fig. 3a). The axial and off-axial topography of the SEIR and the depth of the axial zone vary significantly along its strike (Figs. 2, 3). This is partially related to the existence within it of two areas with an anomalously heated mantle: the ASP plateau, the formation of which is explained by the influence on the ridge axis in this place of the cognominal hot spot [19, 55] and the Keguelen plume [43, 55], and a zone with an anomalously cold mantle—the area of the AAD.

Five provinces can be identified based on the change in axial depth, the morphology of the rift zone, the strike of the ridge, and the nature of its segmentation by morphostructural faults within the SEIR: western, located between the Rodrigues TJ and the ASP plateau; the ASP plateau province, central—between the ASP plateau and the AAD, the AAD province; and the eastern province stretching from the eastern boundary of the AAD to the Macquarie TJ, disturbed by the gigantic system of Tasmantide–Balleny transform faults, which have displaced the ridge axis by almost 1000 km.

In the western province from the Rodrigues TJ to 29.5° S, the ridge has a deep well-formed rift valley 15–20 km wide, with a relative depth of 1000–1500 m (Fig. 2, lines *a*, *b*). Near 29.5° S, the relative depth of the rift valley drops to 200–400 m [43]. These shallower rift valleys are commonly 10–15 km wide, with a topographic amplitude of 100–150 m. In the area of the ASP plateau, the rift valley virtually disappears (Fig. 2, line *c*). In the western extremity of the central province of the SEIR, directly near the ASP plateau, the rift zone has the form of a shallow rift valley, which at about 82° E is replaced by an axial rise that is evidently associated with the influence of the Kerguelen

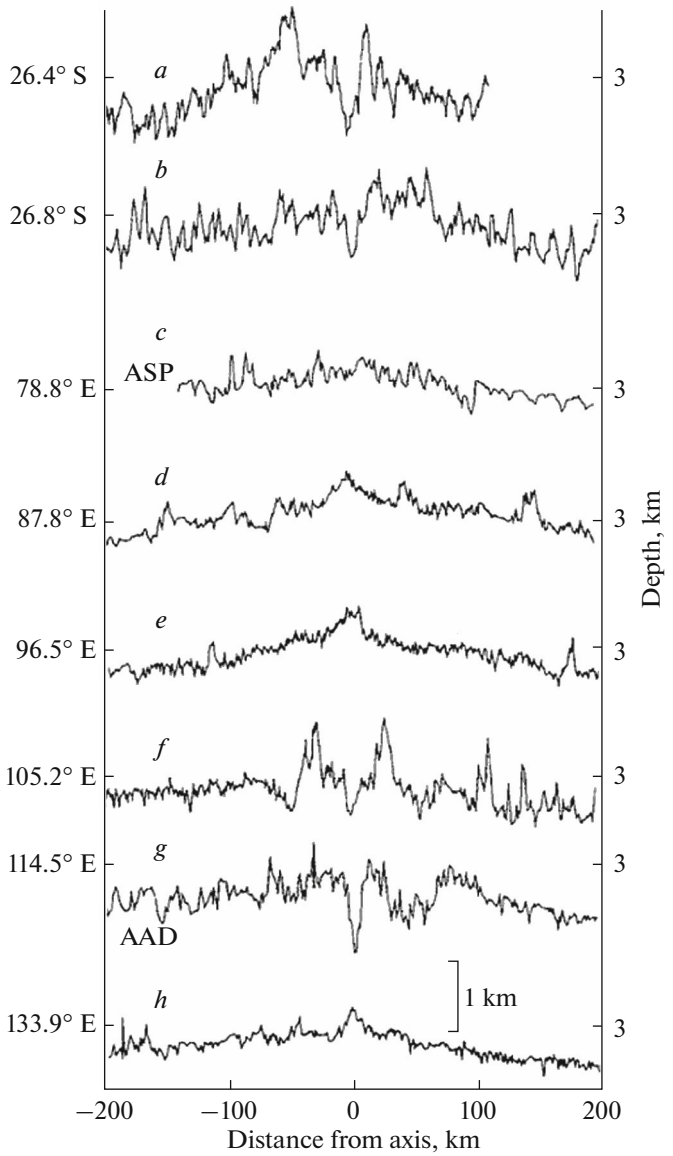

Fig. 2. Cross bathymetric profiles according to [43]. (*a*)–(*h*) Profile marking. ASP is Amsterdam–St. Paul plateau; AAD is Australian–Antarctic discordance.

plume on the SEIR axis there [43] (Fig. 2, lines *d*, *e*). Farther east, the axial rise gradually becomes less distinct and is replaced by rift valleys, which generally deepen towards the AAD (105°–114° E) (Fig. 2, lines *f*, *g*; Fig. 3a). Throughout the length of the AAD province, the rift zone has the morphology of a deep rift valley with an intensely dissected topography (Fig. 3a), and at its eastern boundary, the abrupt transfer of the axial morphology to the axial rise occurs again, which is typical of the entire eastern area of the SEIR (Fig. 2, line *h*). Therefore, the morphology of the rift zone changes several times along the SEIR.

The segmentation in the studied section of the ridge was formed by transform faults (first-order segments according to classification [44]), nontransform offsets (NTOs), propagating rifts, and overlapping spreading centers (second-order segments). According to the scheme adopted in [52] and used later in [17, 19], first-order segments within studied section of the ridge are marked by the letters of the Latin alphabet starting from the Rodrigues TJ, and second-order segments are marked by corresponding letters with numerals. Within the area under study segments from J3 to U are located. The area of the AAD is subdivided into three zones: A, B, and C. East of the AAD, numeration of segment begins again from A (Fig. 2a).

Influence of Amsterdam–St. Paul Hot Spot

The ASP volcanic massif forms a morphologically isolated area covering both the rift zone and the flanks of the SEIR (Fig. 4). The volcanic ridge is located

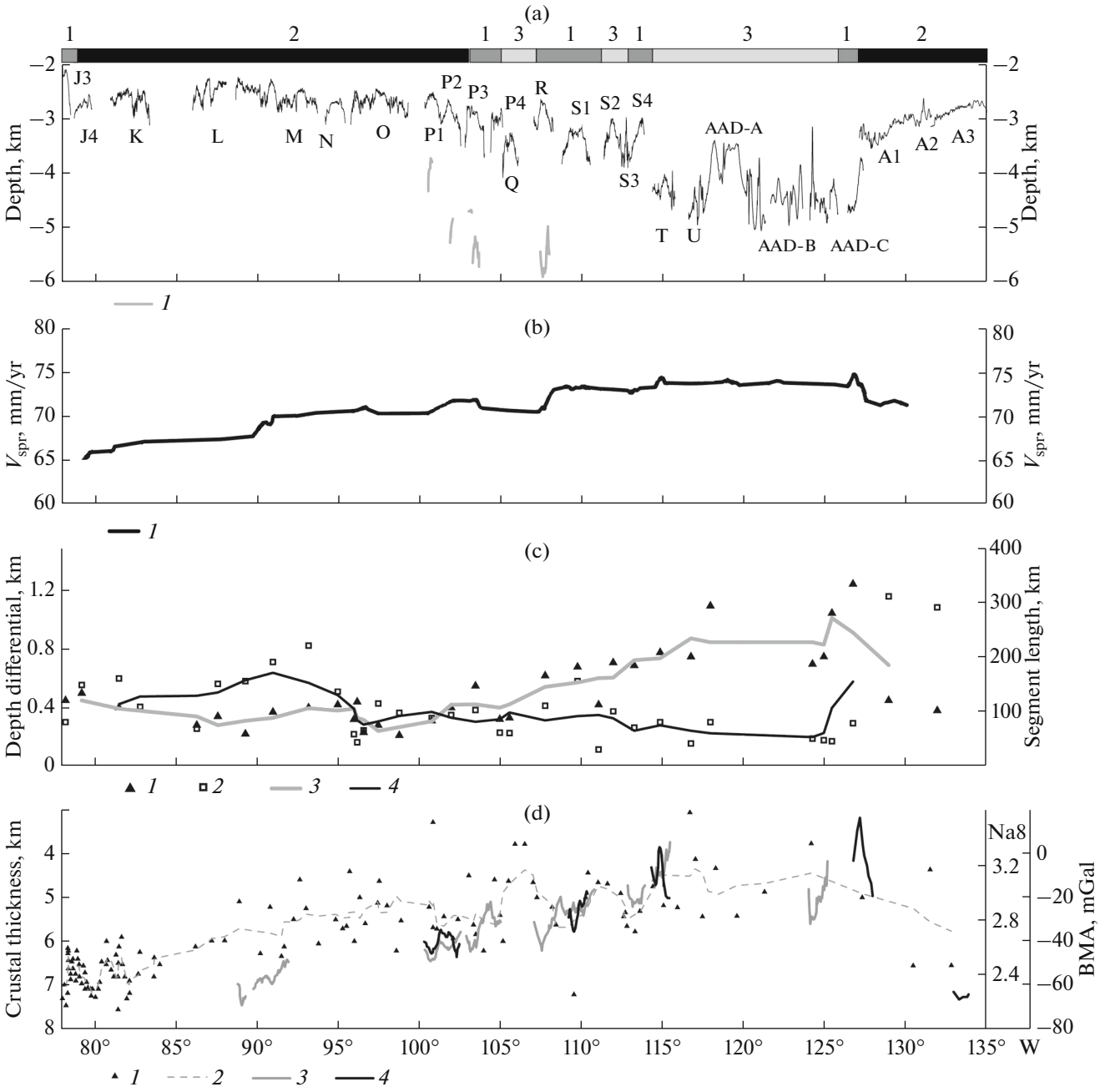

Fig. 3. Changes of ridge structure and spreading rate in section from 78° to 135° E. (a) Bottom topography according to [51, 53]. I–U, A1, A2, A3 is numeration of ridge segments according to [55, 58]. AAD-A–AAD-C are segments of AAD zone according to [41]. Areas with different structure of ridge: (1) transient morphology, (2) axial rises, (3) rift valleys. (*1*) AMC roof according to [12]. (b) Spreading rate according to [22], (1) averaged curve for spreading rate. (c) Changes of segmentation parameters. (*1*) Along-axis depth amplitude, (*2*) segment length, (*3*) averaged curve of depth amplitude, (*4*) averaged curve of segment length. (d) Ridge magmatism. (*1*) Value of Na8 parameter [34, 41, 45], (*2*) averaged curve of Na8, (*3*) gravity anomalies in Bouguer reduction according to [51, 58], (*4*) crustal thickness according to [37].

between two distinct transform faults: Amsterdam and St. Paul. At the intersection with the spreading axis, it forms the ASP plateau, within which the axial depth is about 2300–2800 m. The typical depths in the SEIR segments within the platform are 1–1.5 km smaller than the depth of the spreading segments outside the platform (Fig. 3a), which confirms the formation of a thicker oceanic crust. This also confirms the distribution of gravity anomalies, in particular, the presence of a negative mantle Bouger anomaly (MBA) (e.g., in segment I2, the MBA values reach –100 to –115 mGal); therefore, the average thickness of the platform crust is

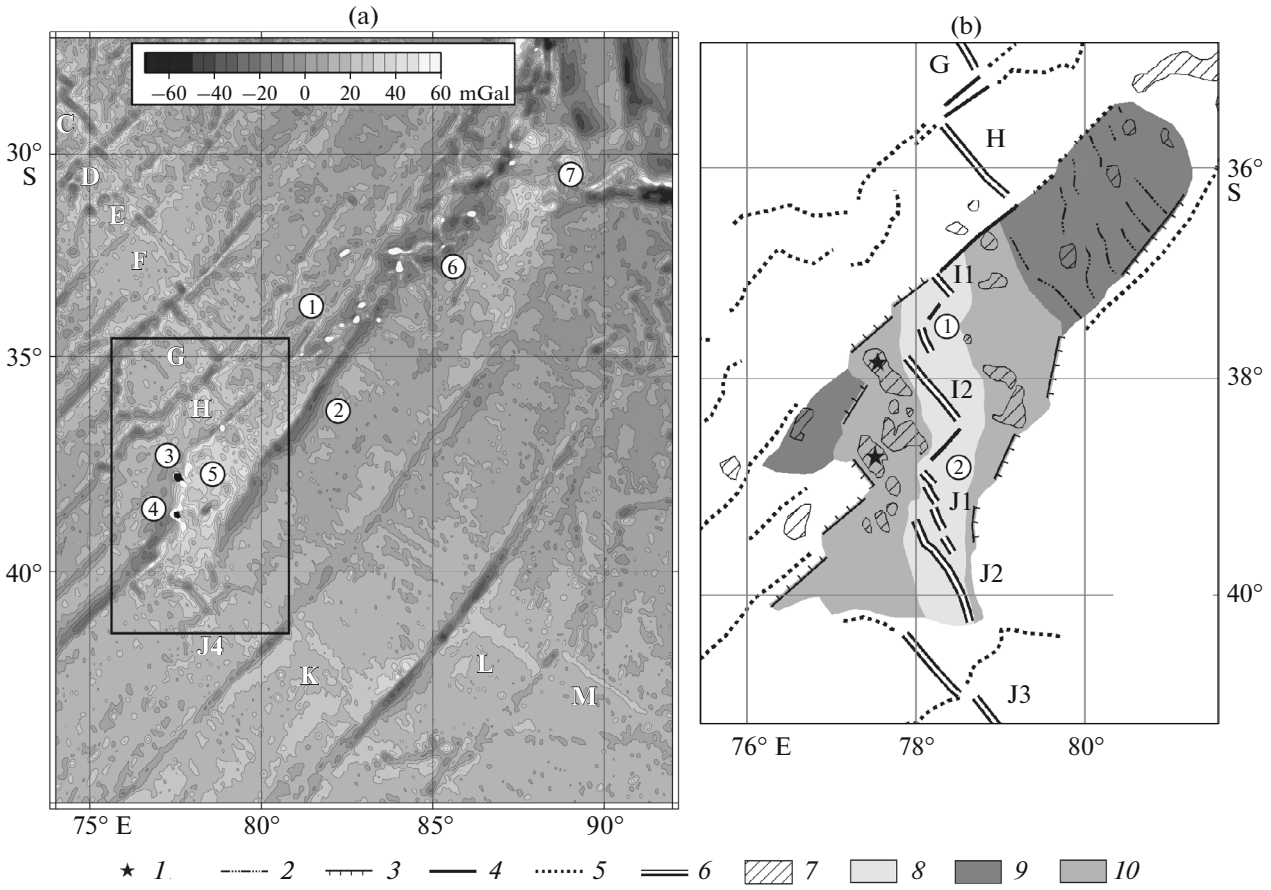

Fig. 4. Amsterdam–St. Paul plateau. (a) Map of gravity anomalies in free air in area of ASP plateau [31]. Isolines are drawn across 50 mGal. A–M is numeration of ridge segments according to [52, 55, 58]. Numerals in circles indicate: (1) Amsterdam transform fault, (2) St. Paul transform fault, (3) Amsterdam Island, (4) St. Paul Island, (5) ASP plateau, (6) Dead Poets seamount chain, (7) Broken plateau. (b) Segmentation of rift axis in ASP plateau surroundings. Arbitrary notes: (*1*) volcanic islands, (*2*) segments of ancient spreading axes according to [46], (*3*) plateau steps, (*4*) active sections of transform faults, (*5*) off-axis traces of transform faults and non-transform offsets, (*6*) spreading segments, (*7*) volcanic edifices, (*8*)–(*10*) stages of plateau lithosphere generation.

about 10 km, which is approximately 40% thicker than typical oceanic crust [55]. Meanwhile, it can reach 12–16 km near the St. Paul and Amsterdam islands.

The minimum Na8 values (the parameter reflecting different Na contents in initial rift tholeiites, which increases with decreasing melting depth), the significant length of segments, the low amplitude of the along-axis topography, and the general morphology of the topography testify in favor of excessive heating of the lithosphere of the rift zone. The transform faults (TFs) on the ASP platform frequently stretch nonorthogonally to the spreading direction: the Boomerang TF is located 14° to the spreading, and the Hillegom TF, 7° (Figs. 4a, 4b). The spreading axis in segment J1 consists of a system of sigmoidal en-echelon fracture systems similar in structure to the segmentation of the northern part of the Reykjanes Ridge, located near the Icelandic plume [25, 57]. The segments significantly overlap each other along the length (Fig. 4). The axes of spreading segments on the ASP plateau moved towards the hot spot by local jumps [46]. The hot spot evidently, at least during the period of its active functioning, "pulled" the rift fracture by repeated local jumps [46]. During periods of fading activity, jumps of the axis ceased and axial rises were replaced by rift valleys. These changes are observed in the topography of the distal part of the plateau [46]. Changes in hot spot activity are noted in the structure of the plateau itself (Fig. 4). The thermal influence of the ASP hot spot leaves a typical trace in the off-axial morphology. This is especially distinct in the segment between the Amsterdam and St. Paul TFs (Fig. 4a). This trace stretches on a significant distance from the spreading axis, fixing the history of the volcanic activity of the hot spot in the seabed topography in the form of the Dead Poets seamount chain [46].

Farther southeast along the strike of the SEIR, the thermal influence of the ASP hot spot in the area of the central province on the topography of the SEIR rift zone weakens. The reduction in thermal influence is reflected in the abrupt deepening of the rift axis at segment J2, about 130 km east of the center of the hot

spot. The depths here increase from 2 to 3.2 km, and the cross profile changes from the axial rise to the reduced rift valley. Segment J3 is characterized by a wide range of topography macroforms—from axial rises to the reduced rift valley with an amplitude of −0.5 to +0.3 km. Reduction in magmatic activity is observed in segment J2, which the local increase of the Na8 indicator up to 2.3–2.5 testifies to. In segment J3, it restores with the reduction of the Na8 indicator up to 2.2–2.4 [34] (Fig. 3b).

Considering the specific features of SEIR tholeiite magmatism, it can be stated that the influence of the ASP hot spot is quite high. This is expressed in the origination of hotter magmas (TOP-1 type) that form at pressures of 20–15 Kbar, a degree of melting of 15–18%, and a temperature interval of 1350–1280°C. Such tholeiites are typical of hotter areas of spreading ridges (MOR areas near Iceland, Azor, Bouvet, etc.) [9]. The primary tholeiite melts of this deeper type in origin have an elevated Fe content and reduced Na content. The diagram (Fig. 3c) that shows variations in the Na8 values in tholeiite glasses (the Na_2O concentration converted to 8% MgO in the melt as per [41]) demonstrates that such magmas with low primary Na_2O values (2.2–2.6) that developed in segments J and K are influenced by the ASP plume. The process of accretion of oceanic crust farther east along the ridge is associated with the generation and fractioning of primary melts (TOP-2 type) according to classification [7], which is typical of all spreading zones of the World Ocean, with the generation of parent magma in the course of fractional polybaric melting of the oceanic mantle in the uprising mantle column at a pressure of 20 to 8 Kbar and temperature T = 1320–1250°C [3, 8]. The Na8 values are in the range of (2.6–2.9).

Influence of the Kerguelen Plume

Farther east the ridge is under the influence of the Kerguelen plume influencing the subaxial mantle of this area at the distance of about 1000 km [43, 55]. According to [56], this value can exceed 1300–1500 km.

About 43–40 Ma ago, the propagation of the SEIR rift fracture to the northwest caused the separation of the Kerguelen plateau and the Broken Ridge [15]. Since then, the active influence of the Kerguelen plume on crustal accretion on the SEIR began and still continues.

The isotopic parameters of basalts of the ASP and Kerguelen hot spots are different, which contradicts the hypothesis of the simple connection at the sublithospheric mantle level of mantle differentiates of a large off-axial Kerguelen plume and the ASP hot spot [50]. The influence of the Kerguelen plume is reflected in the isotopic parameters of the ridge basalts varying eastward, e.g., $^3He/^4He$ [35]. They testify to the maximum heating of the mantle in the area of the L segment at 87°–90° E. The content of Na8 in basalts is minimum in the area of the K segment at 82°–83° E, where it makes about 2.1 and gradually increases eastward (Fig. 3d) [45]. The K–P2 segments are located within the province. The maximum influence of the plume is confirmed by the morphometric data. For segments K, L, and M axial depths of 2.2–2.9 km are typical with a minimim of 2,2 km at segment L2, which is a minimum value throughout the ridge area up to the AAD. The second-order segments here reach a maximum length of 120–160 km. Axial rises with an amplitude of 0.3–0.6 km are typical of these. The amplitude of the along-axis topography is minimum, too: 0.2–0.6 km.

In the eastern direction, the morphometric indicators and the Na8 indicator change, which testifies to the reduction in magmatic activity: deepening of the axis, reduction in segment length, and increase in Na content occur (Fig. 3).

East of 100° E, there is a province with transient morphology, where the segment structure combines all types of topography macroforms of the rift zone. Father east, the axial rises are replaced by rift valleys through areas with reduced and transient forms, and deepening of the axis occurs.

An overall change in the parameters towards reduction in magma supply occurs: deepening of the axis, increase in the amplitude of the along-axis topography, increase in the Na8 indicator, and reduction in segment length.

East of 114° E, there is a province with rift valley morphology. Passing to this province, deepening of the axis by approximately 1–1.2 km occurs, the length of the segments decreases, and the Na8 indicator increases to 2.8–3.6. The morphology of the rift valley with depths up to 4.8 km is typical of segment T. At segment U, located at the western end of the AAD, the relative depth of the rift valley reaches 1.5–2.5 km and the difference in the along-axis topography is 0.9–1.1 km. Meanwhile, axial depths reach 3.8–5 km (Fig. 3a).

Australian–Antarctic Discordance

The AAD province is located between 120° and 128° E (Fig. 1). The length of the AAD province is about 500 km. It occupies the center of the Australian–Antarctic depression between Australia and Antarctica and is one of the deepest areas in the global system of MORs (4000–4500 m) [48]. The AAD province in the west and east is limited by two major transform faults with an axis offset by more than 100 km [48]. At the intersection of the transform fault bounding the AAD from the east, the depth of the bottom (Fig. 3a), the ridge morphology, the amplitudes of magnetic anomalies, seismic activity, and geochemical composition of dredged rocks change significantly. Less distinct changes occur at the intersection of the western boundary of the AAD [48].

Despite the fact that the highest spreading rates at the SEIR are typical of the AAD province, it differs

sharply from other areas of the anomalous deep rift zone and flanks by a rift zone morphology atypical of an intermediate spreading ridge with a deep rift valley; more likely it is typical of slow spreading; it also has a peculiar type of offsets (Fig. 2, profiles *f*, *g*; Fig. 3a). The nature of segmentation of this area varies abruptly as well. In the AAD province, the SEIR is dissected by a dense system of transform faults with large offsets: the length of segments here is anomalously small. The atypical morphology of rift valleys at the AAD as well as the strong degree of dissection of the topography by faults are reflected in the noticeable increase of the topography dissection level in the AAD rift zone. When approaching AAD area, there occur magmas with increased values of Na8 > 3 and less deep tholeiites (Na-type) typical of the coldest provinces of slow-spreading zones similar to the Gakkel and Knipovich ridges, and the equatorial Atlantic [26].

Detail study of the segments in the central part of the AAD in the area of 124°–125°30' E showed the presence of extremely large (in area) internal complexes occupying up to 75–80% of the area of one of the ridge flanks. The largest is located on the Antarctic Plate and completely occupies the southern flank of the rift zone in the area of 124°40'–125°10' E; the sizes of the complex are about 40 km long and 60 km across the spreading axis [51]. Study showed an exceptionally high degree of spreading asymmetry, when up to 80% of accretion during the recent 1.5–2 Ma occurred at one of the ridge flanks. Typical of the segments are minimum MBA values, reaching 0–20 mGal, and the high degree of magnetization intensity at the ridge flanks, presumably testifying to a high degree of rock serpentinization [51]. All of this confirms the exceptionally low value of magmatic activity at this part of the ridge.

East of the AAD, the magmatism intensity increases. The morphology of the axial rise, which is 0.2 to 0.5 km high, and the along-axial depth amplitude of about 0.2–0.4 m are typical of the rift zone. The axial depths increase abruptly up to 2.8–3.2 km. The length of the segments reaches 80–230 km. All morphometrical indicators are similar to those in the areas of segments L and M of the axial rise province. The value of the Na8 indicator falls to 2.4–2.9 (Fig. 3).

ALONG-AXIS CHANGES OF THE DEEP STRUCTURE AND THEIR RELATION TO THE CHANGES OF MANTLE TEMPERATURE

At least three thermal anomalies in the mantle act on the SEIR along its strike influencing its structure and the specific features of magmatism. First, this is the ASP hot spot [19, 55]. Evidently, the increase in mantle temperature approaching this hot spot also partially determines the change in morphology near 29.5° S.

Farther east of this hot spot, at about 82° E, the morphology of the SEIR rift zone is influenced the Kerguelen mantle plume (Fig. 5) [43, 55]. A further change of the morphology of the SEIR rift zone to the east is determined by the gradual cooling of the mantle at the approach to the AAD, where decrease of the mantle temperatures and the crustal thickness, increase of the thickness of the brittle layer in the lithosphere and ruggedness of the seabed topography (Fig. 5) can be expected.

Based on analysis of gravity anomalies in the SEIR rift zone in the area of 88°–120° E and for the ASP plateau, the thickness of the crust was calculated. It decreases in the eastern direction from 10–15 km on the ASP plateau up to 7.5–8 km in the area of 88°–90° E and to 4–4.5 km in the area of 118°–120° E [55, 58]. Crustal thickness measurements obtained with seabed seismometers in the area of 100°–135° E confirmed the calculated values [36, 37]. The measurements were performed along the profiles centered on the ridge axis of segments P1, P2, S1, T, AAD-S, and A3. The measurements showed that the crustal thickness decreases to the east. On average, it is 6.1 (P1), 5.9 (P2), 5.2 (S1), 4.6 (T), 4.9–5.2 (AAD-C), and 7.3 (A3) km. At the AAD-S, the measurements were performed in the eastern extremity on the segment propagating to the west. Here the measurements covered fragments of the lithosphere that formed both at sites associated with accretion under conditions of the well-heated Pacific mantle and in the Indian mantle with a relatively reduced temperature. In the first case, the average crustal thickness was 5.2 km, and in the second case, 4.8 km. Farther east of the AAD, the thickness of the crust abruptly increases.

The thickness of the crust on the ridge flanks in the area of 100°–118° E, obtained from analysis of gravitational data, showed the decrease in the eastern direction from 7–7.5 to 5–6 km and the reduction in mantle temperature in the area of 30°–50° [59]. Meanwhile, estimates of absolute mantle temperature values differ. It is 1320°C in the area of the AAD and ~1470°C in the area of 78°–90° E according to the models in [40] and estimates for mantle depths of more than 250–300 km [21]. Even lower mantle temperature estimates exist for the area of the AAD.

Analyzing the change in geoid height with age, as well as increased S-wave velocities in the upper 200 km of the mantle under the AAD, Marks et al. [49] made the assumption that the upper mantle here is 170°C colder and 0.02 g/cm^3 denser as compared to the normal mantle; i.e., the temperature of the upper mantle is 1160°C. The geochemical trends of the main elements agree with the minor quantity of melting at minor depths, which is good evidence of lower mantle temperatures under the AAD [49]. The Na8 indicator testifies to the change in the degree of melting at minor depths and to a deeper melt (the higher this indicator, the deeper melts are erupted at the surface in the rift zone). This indicator increases towards the AAD, reaches a maximum (Na8 > 3) in its cross section, and

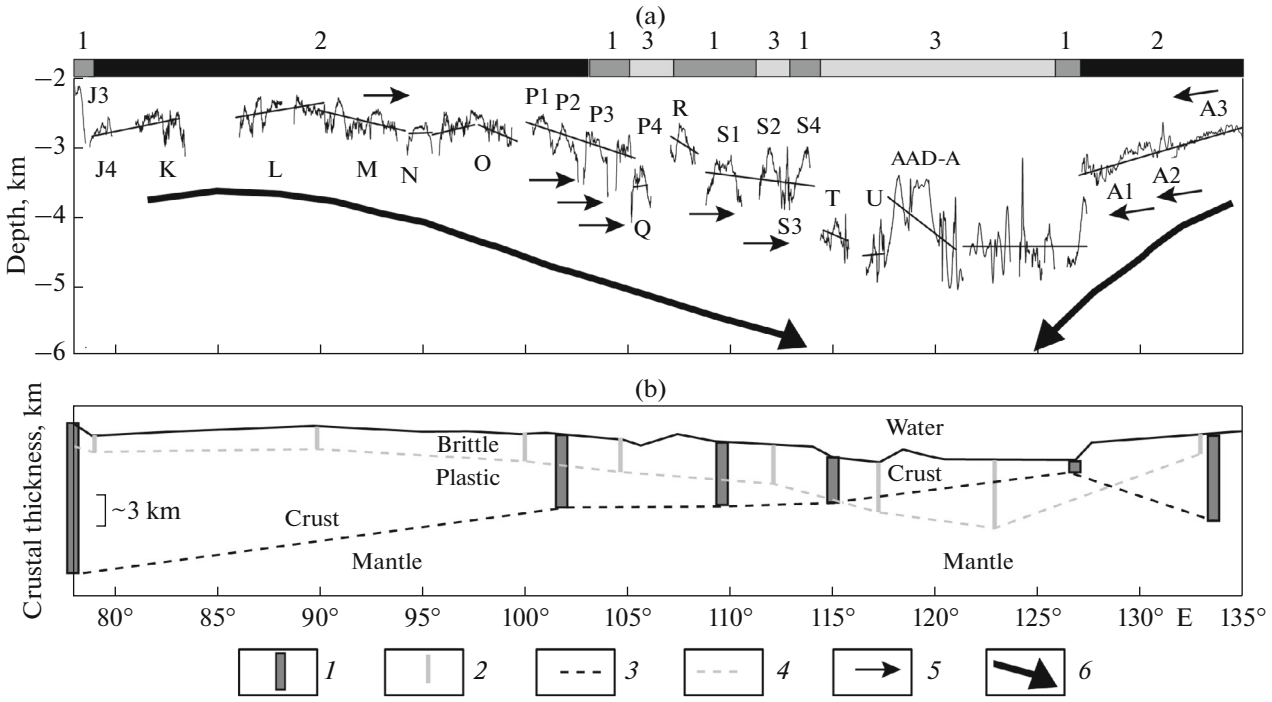

Fig. 5. Influence of along-axis flow on morphology and deep structure of SEIR with account of [58]. (a) Change of along-axis topography. I–U, A1, A2, A3 is numeration of ridge segments according to [55, 58]. Areas with different structure of the ridge: (1) transient morphology, (2) axial rises, (3) rift valleys. (b) Schematic section of rift zone of ridge. Arbitrary notes: (*1*) crustal thickness according to [55] for ASP plateau zone and [37] for the rest of the ridge, (*2*) approximate thickness of brittle layer according to numerical modelling data, (*3*) crust-mantle boundary, (*4*) boundary of brittle-plastic transition, (*5*) location and direction of propagating rifts, (*6*) assumed direction of along-axis flows. Along-axis flow can result in asymmetry and directions of ridge segments propagating.

decreases abruptly to the east of the AAD (Fig. 3c) [34, 41, 45]. This also confirms the reduction of mantle temperatures from west to east along this area of the ridge. The behavior of other elements also demonstrates minimum values of the mantle temperature in the area of 115°–125° E as compared to the other ridge segments and an abrupt increase in temperature east of the AAD [41].

Papers [12, 13] present the results of seismic studies in the axial zone of the ridge. At several segments in the zone with transient morphology, axial magmatic chambers (AMCs) were detected (Fig. 3a). Segments P1, P2, P3, P4, R, and S1 were studied. AMCs were recorded at segments P1, P2, P3, and R. The depth of the AMC roof increases in the eastern direction: 1.5 (P1), 2.1 (P2), 1.9–2.3 (P3), and 2.9 (R1). This parameter correlates well with the structure of the rift zone of the ridge, its axial depth, and the morphometrical parameters of normal faults of the ridge flanks. In the areas of axial rises, the AMC occurs close to the surface; in areas of reduced rises, the chamber deepens. The roof of the AMC under reduced rift valleys was observed in a small area in segment P3. Here the AMC roof abruptly deepens on 300 m. Deepening of the along-axis profile on 250 m is observed as well. Moreover, the roof stairly deepens in the western part of the segment upon transitioning from the axial rise to a reduced axial rise on the depth of about 600 m. In the area of segment R, the AMC is also traced only within the length of the axial rise and abruptly deepens in areas with reduced rises and transient morphology. Areas with the minimum depth of AMC formation are characterized by geophysical and morphological indicators testifying to increased magmatic activity. The minimum dissection of the off-axis topography [33], small anomalies in the Bouguer reduction [58], and increased values of crustal thickness obtained from gravity data are typical of them [59]. All these indicators change abruptly in zones of reduced magma supply, where deepening and disappearance of the AMC and transition from the morphology of axial rises to transient forms of the rift zone morphology are noted. Deepening of the AMC roof in the eastern direction can be related to the regional trend of reduction in mantle temperature and crustal thickness. It is evident that the presence or disappearance of the AMC controls the rheological structure of the crust in the rift zone of the ridge and, accordingly, the accretion regime of the crust and the topography of the rift zone and ridge flanks [3].

Therefore, the along-axis asthenosphere flow occurs in the area of the central province of the SEIR

located east of the ASP plateau (Fig. 5). It is mostly formed by the Kerguelen plume and, to a lesser extent, the ASP hot spot. The migration of Kerguelen plume material towards the spreading ridge can occur along the channel or along the base of the lithosphere, the level of which increases towards the spreading axis [38, 55]. This flow moves east towards the AAD, under which there is an area of relatively cold mantle [58]. The existence of the along-axis asthenospheric flow and the assumed reduction of its intensity to the east can have a number of observed consequences. These are the direction of development of propagating rifts, reduction of the axial depth from west to east, wedging out of AMCs, increase of the value of the brittle lithospheric layer and decrease of the crustal thickness in the deep structure; change of the axial morphology from the axial rise with the segmentation of long segments and overlapping-type offsets of spreading axes through the transient type of the morphology to the rift valley with the segmentation of short segments by faults of the nontransform-type offsets in the topography of the rift zone (Fig. 5).

The presence of the anomalous AAD structure in the area of the relatively cold mantle has both genetic and geodynamic causes. The prebreakup heterogeneity of the Australian–Antarctic lithosphere and the presence of the Gawler–Mawson craton, which represented a thick structural–rheological barrier to development of the rift zone, evidently played an important role [11]. On the other hand, this area represented an accommodation zone separating the Pacific and Indian Ocean provinces of the tectonosphere, which evidently differed in their tectonophysical parameters (mantle heating, lithosphere thickness, asthenospheric viscosity, etc.), for which development of rifting and further spreading processes had different dynamics and kinematics that determined the direction and intensity of asthenospheric flows (Fig. 6).

INFLUENCE OF MANTLE TEMPERATURE VARIATIONS IN HOT AND COLD ZONES OF THE MOR ON THE THERMAL STRUCTURE OF THE RIFT ZONE AND ITS MORPHOLOGY (NUMERICAL MODELLING)

The influence of mantle temperature anomalies caused by the presence of relatively hot and cold zones on the thermal structure of the SEIR was studied by numerical modelling of the spreading process. We used a nonstationary numerical model of discrete-continuous spreading assuming the formation of a crustal layer in the oceanic lithosphere as a result of repeated intrusions of the melted material at the spreading axis. The frequency of intrusions (spreading episodes) in the model depended on the spreading rate. The balance of heat flow from intrusions and its diffusion through conductive and hydrothermal (convective) cooling mechanisms determine the depth and the shape of magmatic chambers in the model. The temperature of the mantle in the basis of the model area of calculation varies from 1150 to 1350°C, which makes it possible to analyze areas with a hot and cold mantle.

A detailed description of the model is given in [29]. The model allows calculation of the thermal structure of the lithosphere and alteration of the degree of rock melting under MOR rift zones at variable spreading and mantle temperature rates. The result of numerical modelling is the depth pattern of the thermal state of rocks, reflecting the location, shape, and sizes of melting chambers in the crust and the subcrustal mantle right under the spreading axis and at different distances from it. Estimates have shown that the spreading rate is the determining parameter in the formation of the thermal structure of the rift zone (Fig. 6).

For fast-spreading ridges (e.g., the East Pacific Rise), numerical experiments demonstrate the existence of stationary magmatic chambers at the upper-mantle level with the roof at the Moho boundary and at the crust level with the magmatic chamber roof at depths of ≤1.5 km (Fig. 6d). An area of focused mantle upwelling with increased melt concentration in the mantle forms at low spreading rates (Fig. 6a). The situation changes depending on the degree of heating of mantle rocks. The area of melt concentration either remains in the mantle or is uplifted to the crust–mantle boundary or even penetrates the crust, forming local short-living magmatic chambers in it (Fig. 6b).

The transient situation between slow and fast spreading rates is the most interesting for the area under study. When the spreading rate increases, intrusion frequency also increases, the mantle heating in the axial zone intensifies, and the depth of the roof of the melt zone decreases, thus reaching the Moho boundary. The melt concentrates at the crust–mantle boundary, and an upper mantle magmatic chamber (or melt lens) under the crust is formed. A further increase in the spreading rate above some boundary value of about 4–5 cm/yr for a mantle temperature of 1250°C leads to the formation of a stationary magmatic chamber in the crust of yet insignificant width (Fig. 6c). With an increase in the spreading rate above the specified limit, the melt concentration in the chamber increases. Meanwhile, the depth of the chamber roof will decrease. For example, at a spreading rate of 6–7 cm/yr (Fig. 6c), this is 2.5 km, while at 9–10 cm/yr, it is ~1.5 km (Fig. 6d) [3, 29]. The melt concentration is maximum in the upper part of the chamber where a structure like a melt lens forms. The degree of melting here reaches ~55% at a spreading rate of 6 cm/yr and 95% at a rate of 10 cm/yr. In the lower crust, near the Moho boundary, the melt content drops to several percent. The formation of a stationary melting chamber in the crust is accompanied by simultaneous expansion of the zone of focused mantle upwelling and the formation of a distinct

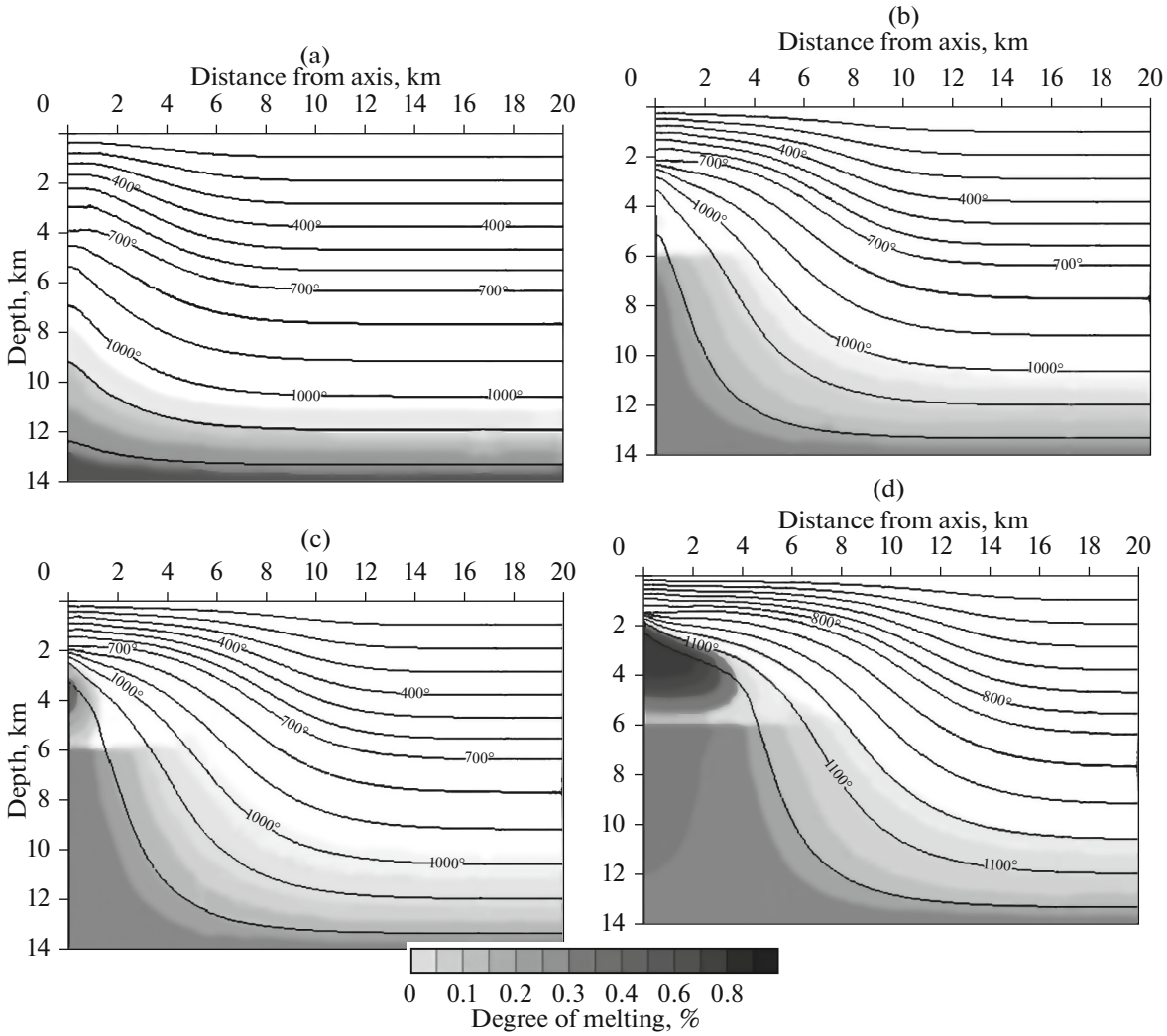

Fig. 6. Thermal structure and distribution of share of rock melting in surroundings of axial zone of spreading ridges [30]: (a) for spreading rate values of 2 cm/yr, (b) 5, (c) 6, and (d) 9 cm/yr.

chamber in the mantle with the maximum concentration of the melt near the Moho boundary.

In [29], we demonstrated that the spreading rate here is an important parameter determining the topography of the axial spreading zone and the nature of the distribution of magmatic chambers in the crust and in the subcrustal mantle.

Let us now consider changes in the thermal structure of the axial lithosphere and in the state of magmatic chambers caused by a change in mantle temperature along the strike of the axial zone of the SEIR at the same spreading rate (Fig. 7). The calculations for the axial zone of the intermediate spreading ridge (V_{spr} = 6–7 cm/yr) at various temperatures of the intruding melt assume that for an increase of mantle temperature by 50–100°C (e.g., in the zones influenced by hot spots), the cross sizes of the crustal magmatic chamber increase (from a halfwidth of 1.5 km at 1250°C to 3 km at 1350°C); the share of the melt in the chamber alo increases. The thermal structure of the axial zone becomes similar to the structure of fast spreading ridges (Fig. 7b, *a*, *b*). A decrease in the typical mantle temperature by 50–100°C leads to a decrease in the sizes of magmatic chambers and the melt concentration in them up to complete disappearance of the crustal magmatic chamber with a mantle temperature of 1200°C or less. This is observed despite significant spreading rates (Fig. 7b, *c*, *d*). Meanwhile, the thermal structure of the axial zone approaches the structure of slow and even ultraslow spreading ridges.

Variations in mantle temperatures and their influence on the deep structure of the crust and the bottom morphology of the rift zone are especially noticeable in areas influenced by hot spots and cold zones. For example, along the strike of the SEIR where changes in spreading rate are insignificant, the morphology changes to the formation of axial rises in areas influenced by the ASP hot spot and the Kerguelen plume are observed. Meanwhile, in the area influenced by

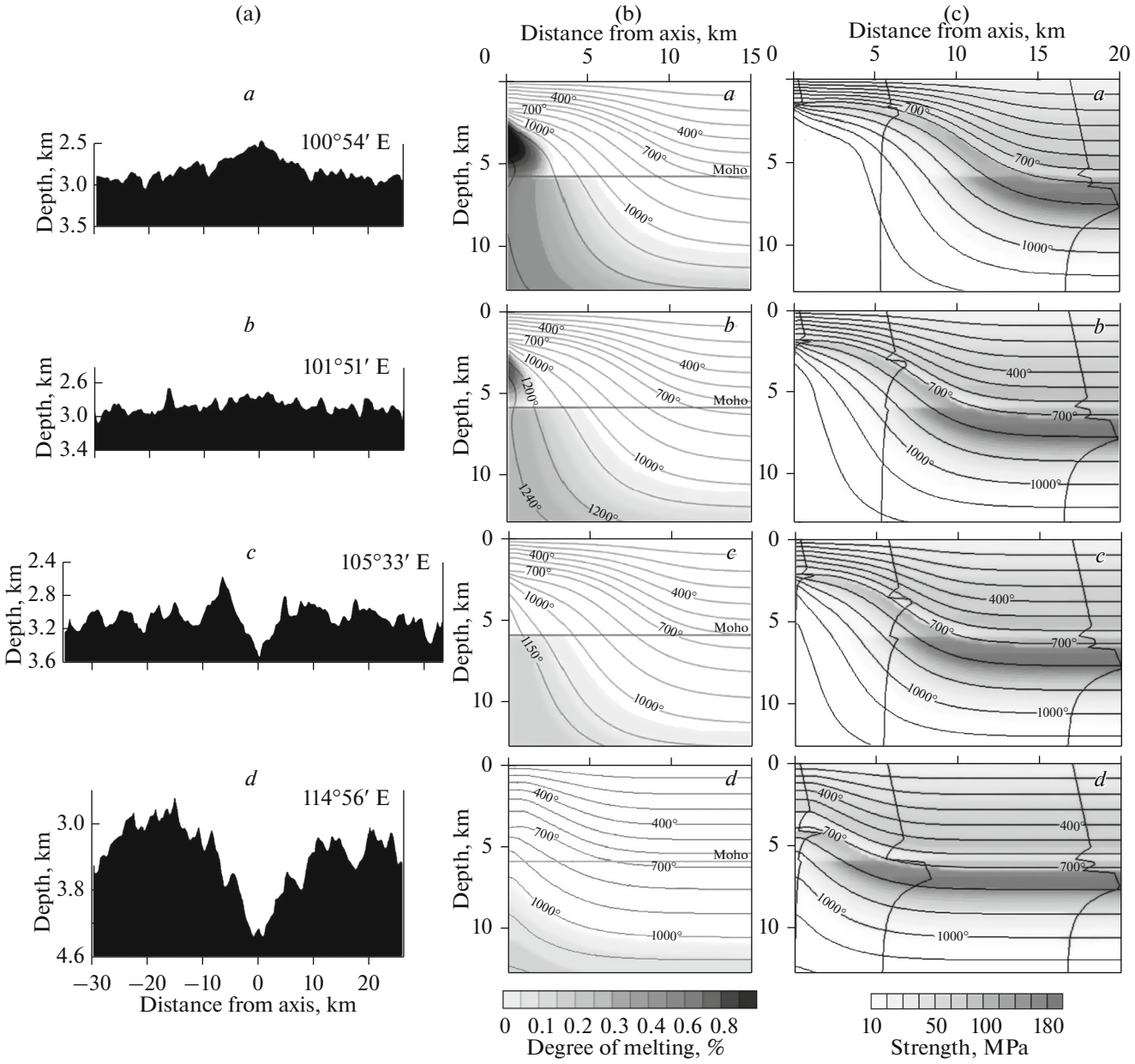

Fig. 7. Relation of axial morphology with thermal regime of SEIR axial zone: (a) change of morphology of rift zone along SEIR strike according to [17]; (b) thermal structure and distribution of degree of melting in axial zone of the ridge at intermediate spreading rate (V_{spr} = 6 cm/yr) calculated for different mantle temperatures. TM = 1300° (*a*), 1250° (*b*), 1200° (*c*) and 1150°C (*d*). Quasi-steady chamber in crust of such MORs disappears at mantle temperature of TM ≤ 1200°C. Increase in mantle temperature leads to increase of sizes of chambers and degree of melting; (c) distribution of strength on background of isotherm distribution. Curves of change in strength with depth are given for distances from ridge axis of 0, 5.5, and 16.5 km. (*a*)–(*d*) Correspondence of typical axial morphology to thermal regime of axial zone and lithosphere strength for different parts of SEIR with different mantle temperatures.

the relatively cold part of the AAD located distally from hot spots, a transition to rift valley morphology is observed. It is remarkable that the rift valleys at the SEIR form in the area with the highest spreading rate of about 75 mm/yr, while the formation of axial rises occurs at lower spreading rates (about 68 mm/yr). This contradicts the known global pattern according to which axial rises are formed at MORs with fast spreading rate and the rift valley is formed at MORs with the slow spreading rate. Therefore, the following conclusion can be made: the changes in morphology of the axial zone of the ridge within the SEIR are associated not with differences in the spreading rate, but with regional changes in the characteristic mantle temperature.

As noted above, changes of mantle temperature can lead to not only a change in axial morphology, but

also to a change of the average depth of the axial zone. An increase of the temperature of the subaxial mantle causes a decrease of the depth of the axial zone of the ridge. For example, the depth of the axial zone increases on 2100 m (Fig. 3a) from areas with a hotter mantle in the zone of the Amsterdam–St. Paul plateau in the eastern direction to the anomalously cold mantle (AAD).

A change in the thermal structure of the SEIR rift zone causes changes in the strength of the axial and off-axial lithosphere, as well as in the nature of the change in topography forming deformations (Fig. 7c). This is evident from a comparison of the poorly dissected topography in the axial zone of the ridge in the area of influence of the ASP hot spot, which testifies to the low strength of the lithosphere with the AAD area, where the strongly dissected high-amplitude topography testifies to the deformation of the colder, stronger, and thicker lithosphere; the significant thickness of the brittle layer determined by the 725°C isotherm.

Analysis of the thermal model of the lithosphere in the SEIR axial zone using the nonstationary spreading model allows numerical estimation of rock strength variations in the young oceanic lithosphere, which is especially important in zones of thermal anomalies associated with the presence of hot spots and relatively cold mantle zones. The rock strength of the lithosphere is estimated using rheological laws connecting brittle and viscous-plastic rock deformations in the oceanic lithosphere with stresses. These laws were obtained during experiments with brittle and plastic deformations of crust and mantle rock specimens [14, 29, 30, 39].

Modelling performed for different temperature gradients and different values of the crustal thickness showed that a narrow zone of viscous-plastic deformations develops directly above the 725°C isotherm (closure temperature for microfractures) [29, 30]. The calculation results confirmed that the $T \approx 725$°C isotherm controls the transition from elastic deformations to viscous-plastic ones in the first approximation. According to the calculations in Fig. 7c, the thickness of the layer with elastic rock deformations increases as a function of mantle heating from the values of 1.5–2.5 km on the ridge axis in areas exposed to the influence of the ASP hot spot and the Kerguelen plume (Fig. 7c, *a*, *b*) to 3–5 km for the relatively cold mantle in the area of the AAD. As the lithosphere cools, the rock strength increases, up to 5–7 km at a distance of 10–15 km from the spreading axis and up to values of about 20 km for the lithosphere with an age of 10 Ma. In the area of the $T \approx 725$°C isotherm, a weakened layer with viscous-plastic rock deformation is evident. This layer, while being thin at the MOR axis, gradually thickens to 1–1.5 km at some distance from the axis, where the 725°C isotherm, while deepening, reaches the mantle roof. Below this weakened layer is another zone of elastic deformations of mantle rocks (or lower crust).

The model estimates showed that tectonic stratification of the oceanic crust and the lithosphere are governed by its rheological stratification, which at the same spreading rate depends on the mantle heating, the thickness of the crust, and its composition [30]. Modelling shows that in the event of a strongly heated mantle, an elastic deformation layer occurs within the mantle only at distances of 10–15 km from the ridge axis (Fig. 7c, *a*, *b*). Meanwhile, in the relatively cold AAD area, a zone of brittle rocks begins almost immediately from the ridge axis, and the topography of abyssal hills along the slopes of rift valleys is formed during downthrow movements of the blocks along the normal faults as the relatively strong lithosphere is stretched. The activity of such faults diminishes on distances of 10–15 km from the axis. Respectively, the relatively high values of the effectively elastic thickness of the axial lithosphere at reduced mantle temperatures are reflected in the appreciable width of the rift valley, in the significant downthrow amplitudes, and accordingly, in the strong dissection of the rift zone topography [28].

The specific features of the crustal and mantle rock strength distribution wit depth and along and across the strike of the SEIR axis significantly depend on the degree of mantle heating, the presence of magmatic systems of different levels, crustal thickness, etc. In different geodynamic spreading conditions of the crust, both one and several levels of strength reduction can be observed, forming a natural rheological stratification of the crust and significantly influencing the levels of in-crust stresses and possible tectonic thrusts.

The numerical modelling results show that at ridges with intermediate spreading rates and transient morphology, the magmatic chambers according to our estimates are commonly present in the crust, but their sizes are significantly smaller than for fast spreading ridges with the axial rise morphology. The stability in time and sizes of crustal magmatic chambers at intermediate spreading rates can change very quickly depending on the change in typical mantle temperatures. Even minor changes in these parameters caused, e.g., by the influence of hot or cold spots and/or structural discontinuities such as transform faults can lead to an increase in the sizes and magma saturation of magmatic chambers or, vice versa, to the disappearance of the chamber and a change in the effective strength of the lithosphere.

Therefore, at intermediate spreading rates (6–8 cm/yr) typical of the SEIR and increased mantle temperature largely controlled by the proximity of the Kerguelen and ASP hot spots, significant changes occur in the crustal accretion mechanisms, thermal and mechanical properties of the crust and lithosphere, the shape and sizes of axial magmatic chambers, and accordingly, the bottom morphology of rift

zones changing from axial rises to rift valleys. In the case of reduced mantle temperatures (in the area of the AAD), crustal thickness decreases, the thickness of the lithosphere increases, brittle layer thickness increases, and a strongly dissected topography with an overdeepened rift valley forms.

FORMATION OF ANOMALOUS TOPOGRAPHY IN HOT AND COLD AREAS OF THE SOUTHEAST INDIAN RIDGE (PHYSICAL MODELLING)

Despite the fact that the numerical modelling results explain real natural situations to a large extent, their comparison with specific natural structures shows that the latter are more complex than those provided in the models. Analysis of natural processes in rift zones requires joint consideration of the thermal evolution of the lithosphere and deformation of the tectonic setting. Therefore, here we mean the thermomechanical processes in the lithosphere and the upper mantle. This is the approach we used for the modelling.

The experiments were performed in a textolite tank with a piston driven by an electromechanical drive. The uniform temperature field of the model substance is ensured by heaters located inside the device. The electromechanical drive makes it possible to vary the deformation rates of the model plate and change the direction of stretching, thus forming conditions of orthogonal, oblique, or irregular spreading. The change in cooling duration provides different ratio of the brittle and plastic lithosphere layers [32].

The substances used in experiments were colloid systems prepared from liquid (mineral oil) and solid (ceresin, paraffin) hydrocarbons, finely dispersed powders, and surfactants. They have elastic–viscous–plastic properties and ensure similarity of model processes to natural ones in terms of the yield limit. Different properties of the material corresponding to the similarity requirements can be achieved by varying values of temperature, deformation rate, and percent ratio of components [10, 60].

The main similarity criterion used in the experiments is

$$\Omega = \tau_s/\rho gH) = \text{const},$$

where τ_s is the shear strength of the model material, ρ is the density, g is gravitational acceleration, and H is the thickness of the model lithosphere.

The purpose of physical modelling was to identify the specific features of the geometry and segmentation of rift fracture and crustal accretion under the influence of thermal anomalies caused by a relatively heated (hot spot) and relatively cold mantle. Conditions similar to the SEIR interaction with the ASP hot spot and AAD area were studied in the experiments.

In preparing the experiments, the model substance was heated with heaters to the required temperature (~43°C) and was brought to a homogeneous liquid state by stirring. Then, the surface of the melt of the model substance was cooled from above with a fan, while a specific thermal regime was maintained inside the setup. The model substance solidified to the required thickness, which simulated the lithosphere, which was welded to the piston and the opposite wall of the setup. Different types of heterogeneities formed in it in some experimental series by a mechanical method: sections, rift fractures, weakened zones with a thinner model lithosphere, or structural inhomogeneities with a stronger and thicker model lithosphere with various configurations, etc. [32]. After the model plate reached the thickness H required for this experiment, horizontal stretching commenced.

The modelling was performed for three experimental series (Fig. 8): (1) influence of the hot spot on the development of the spreading axis and oceanic crust accretion; (2) influence of the hot mantle on the axial segmentation and accretion of the oceanic crust; and (3) influence of the hot spot on the spreading geometry and crustal accretion in the presence of structural heterogeneity with the relatively cold mantle.

The hot spot was simulated by a local heating source (LHS) fixed to the bottom of the experimental setup: ceramic plate ~3.5 x 2.5 cm in size with controllable heating. Originally the thermal influence of the hot spot on the lithosphere surface covers an area 100 to 1000 km across. The thickness of the lithosphere in the axial rift zone is several kilometers. The thickness of the model lithosphere is several millimeters. Therefore, in the model we observed that the spatial sizes of the influence zone of the LHS were one or two orders of magnitude larger than the thickness of the model lithosphere.

Below we describe several experiments from the series along with the main results.

Influence of the Hot Spot on Accretion of Oceanic Crust for the Initial Localization of the Rift Fracture

In all experimental series, the variable parameters of the model included: stretching (spreading) rate V, thickness H_2 of the model lithosphere in the axial zone of the rift, distance from the rift zone to the LHS projection onto the surface of the $L_{rift-LHS}$ model at the beginning of the experiment, time of switching-on of the LHS after the beginning of stretching t_{LHS} and the degree (voltage supplied to it in volts) of its heating U_{LHS}.

Experiment 1 no. 509 (Fig. 9)

After the model plate reached the required thickness, a cut was made in it to the entire depth and length at ~45° to the surface. It was located under the left margin of the LHS, which was switched on immediately after the beginning of stretching. An increase of

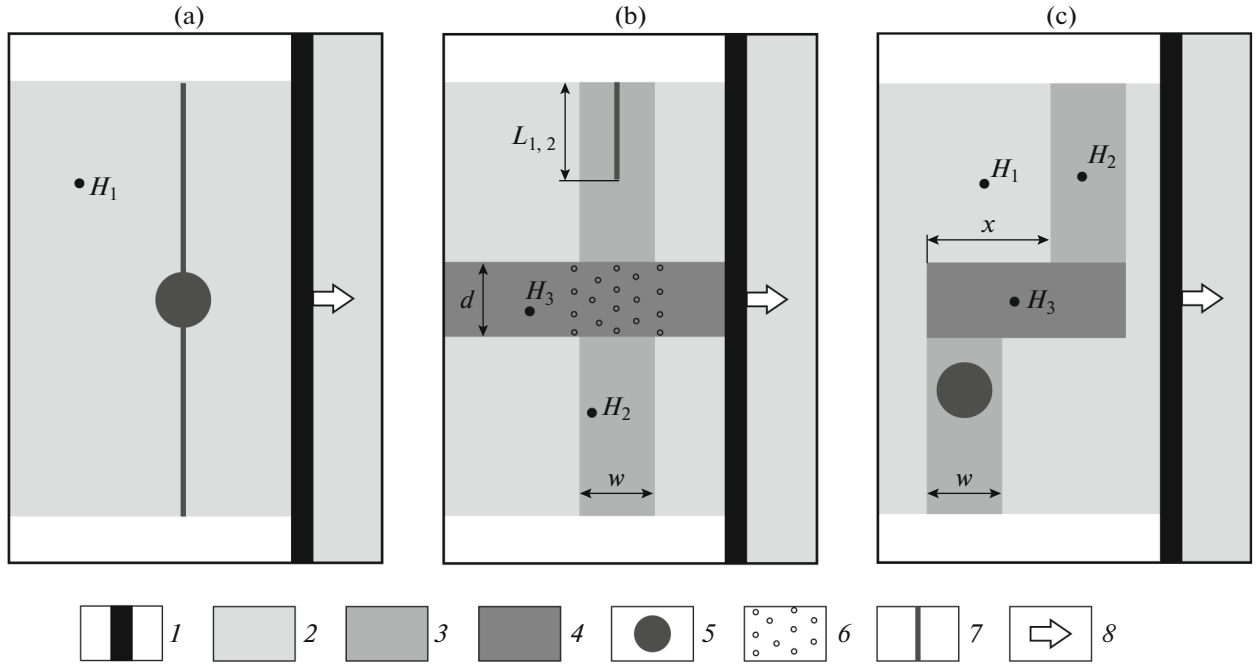

Fig. 8. Layouts and parameters of experimental series (a–c): (*1*) piston; (*2*) model plate, (*3*) weakened zone, (*4*) inhomogeneity with large thickness, (*5*) LHS position, (*6*) area of cooling with water, (*7*) cuttings, (*8*) direction of stretching. $L_{1,2}$ is section length (axes of rift zones); $H_{1,2,3}$ is thickness of surrounding plate, weakened (thinned) rift zone, and structural inhomogeneity with a thicker and colder lithosphere, respectively; *w* is width of weakened rift zone; *d* is width of structural inhomogeneity; *x* is cross offset between cuttings or weakened zones.

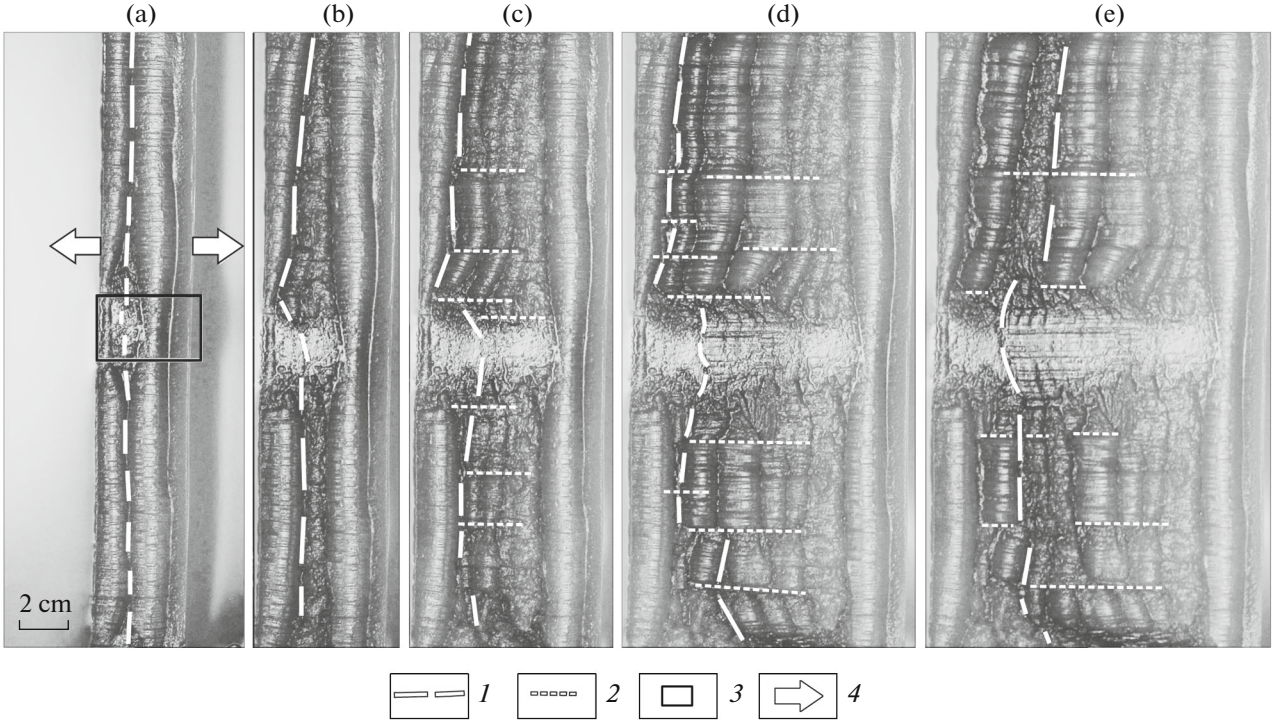

Fig. 9. Experiment 1 no. 509. Evolution of topography in model with hot spot located on axis of rift zone. $V = 1.67 \times 10^{-5}$ m/s; $H_1 = 3 \times 10^{-3}$ m; $L\text{rift}_{-\text{LHS}} = 0$; $t_{\text{LHS}} = 0$; $U_{\text{LHS}} = 140–135$ v. (a)–(e) Experimental stages. Photograph, plan view. White rectangle at Stage (a), LHS projection onto model surface. Arbitrary notes: (*1*) Spreading axis, (*2*) cross faults, (*3*) projection of local heating source (hot spot) onto model surface, (*4*) stretching direction.

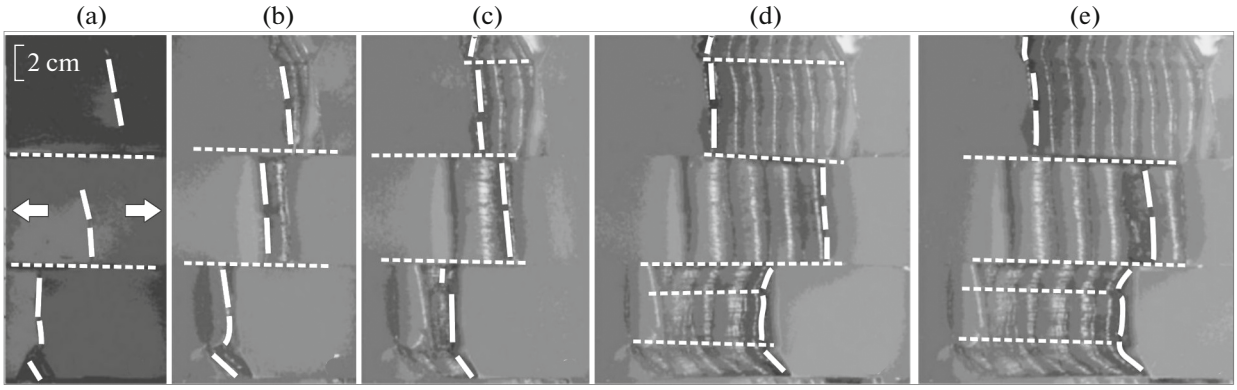

Fig. 10. Experiment 3 no. 1347. Dynamics of fracture development during interaction with stronger and colder block. $V = 1.67 \times 10^{-5}$–3.75×10^{-5} m/s, $H_1 = 3 \times 10^{-3}$ m, plate 0.19 × 0.16 m, $L_1 = L_2 = 2 \times 10^{-2}$ m, $x = 4 \times 10^{-2}$ m. (a)–(e) Experimental stages. Photograph, plan view. For legend, see Fig. 9.

the model crust associated with lithospheric wedge deformations occurred during stretching [47, 60]. On the surface of the model, such deformations are represented by swell-like rises separated by downfolds. In the beginning, the spreading axis was located to the left of the LHS (Fig. 9a). However, after the LHS reached full heating power and locally changed the thermal regime of the model lithosphere, the spreading axis started migrating towards the thermal anomaly and gradually occupied the position above it (Figs. 9b, 9c). The photograph shows that the amplitude of the topography reduces in the influence zone of the LHS due to thinning of the model plate. Some time later, heating of the LHS (the mantle temperature in the hot spot area) was decreased, and this immediately influenced the amplitude of the topography (Figs. 9d, 9e). It began to increase. By the end of the experiment, shallow topography belts—traces of LHS (hot spot) influence on the newly formed crust—were distinct on the model surface. The results of the experiments show good illustration of the conditions of formation of the off-axis ridge as a result of interaction of the ASP hot spot with the SEIR rift zone (Fig. 4).

Influence of Structural Inhomogeneity with Thicker and Colder Lithosphere on the Development of Rift Fractures and Crustal Accretion

Two methodological approaches were used to form the structural inhomogeneity with a stronger lithosphere. In the first, the entire suitable model lithosphere except for the marked block was "cut out." If a weakened zone of width w was formed in the experiment, then the inhomogeneity in the form of a block with increased thickness H_2 and strength was formed within it. The parts of the cut-out plate were removed, and the melt was left in its place. Then, cooling of the model continued; accordingly, the block continued growing and the model plate was formed around it anew. As a result, the thickness of the structural inhomogeneity in the model was greater than the thickness H_1 of the plate surrounding it.

The other approach to increase the strength of the structural inhomogeneity is to cool it with water at room temperature from above (from the surface). This led to its additional cooling and an increase in strength and thickness. This procedure was applied in cases when the increase in thickness (strength) of the model lithosphere by prolonged cooling was impossible due to the geometric features of the model.

Experiment 3 no. 1347 (Fig. 10)

Weakened zones were located in the upper and lower parts of the model plate and were shifted in relation to each other in the stretching direction at $x = 2.5$ cm. In plan view, the upper weakened zone was shifted to the right with respect to the left. In between them, in the middle of the plate, there was a block with a thicker and stronger lithosphere, oriented in parallel to the stretching direction. In the process of stretching, rift fractures formed in weakened zones, which, while approaching each other, reached the strong block. It then split in the middle in the area of offset between the upper and lower rift fracture and formed a new rift segment (Fig. 10a). When stretching continued, the accretion of the new model crust occurred at all three spreading segments offset in relation to each other along the strike-slip faults (Figs. 10b, 10c, 10d). Meanwhile, the accretion in segments was asymmetric. As a result, the axes of spreading segments moved in different directions. The upper segment was shifted to the right, and the lower and the middle segments that formed on a stronger block were shifted to the left. As a result, the configuration of the spreading segments became the following by the end of the experiment. The upper segment occupied the extreme left position, the middle (on the strong block) occupied the extreme right position, and the lower segment was located between them. The segments were separated by strike-slip

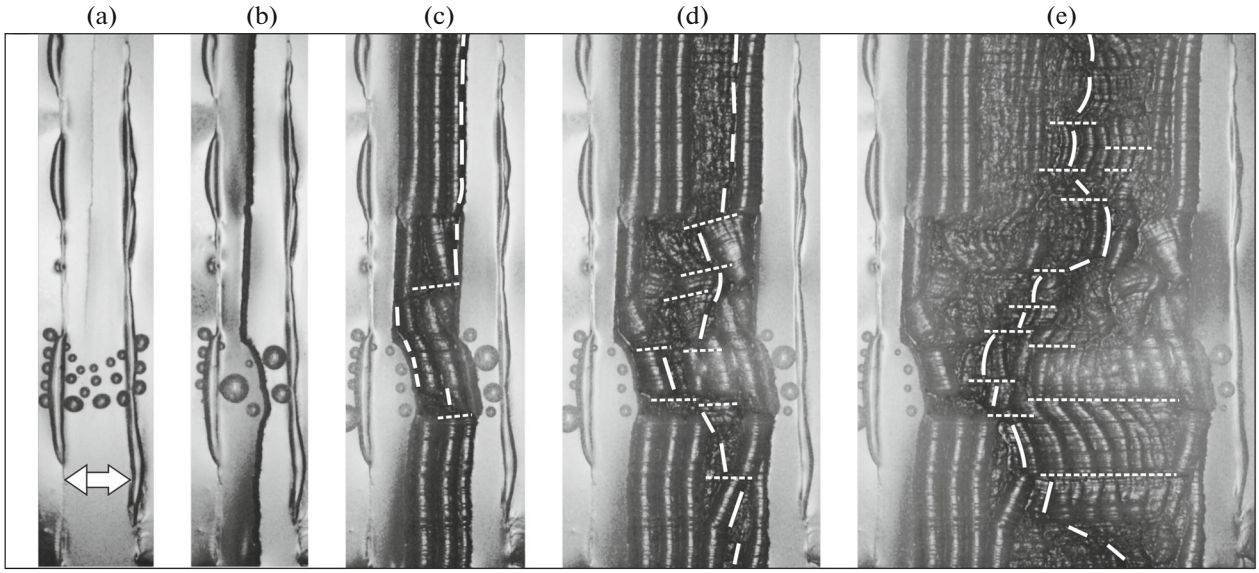

Fig. 11. Experiment 4 no. 1661. Dynamics of fracture development during interaction with stronger and colder block. $V = 2.15 \times 10^{-5}$m/s, $H_1 = 3 \times 10^{-3}$ m, $H_2 = 2 \times 10^{-3}$ m, $w = 3 \times 10^{-2}$ m, plate 0.12 × 0.4 m, $L_1 = 10^{-2}$ m. (a)–(e) Experimental stages. Photograph, plan view. For legend, see Fig. 9.

faults of transform type (Fig. 10e). The model crust that formed on a stronger lithosphere was characterized by a more significant topography amplitude as compared to neighboring segments.

Experiment 4 no. 1661 (Fig. 11)

In this experiment a weakened zone with a thinner lithosphere was set for localization of the rift fracture on the model lithosphere. Its strike was perpendicular to the stretching direction. In the weakened zone, there was a cooled block with a thicker H_3 lithosphere. The increased thickness of this model block was achieved both by its longer cooling and additional cooling with water from above (Fig. 11a). In the upper part of the weakened zone, a 10-cm-long cut was made. A fracture developed in it during stretching downwards until it reached the strong block (Fig. 11a). Here it slowed its development and then crossed the strong block, bending and losing its linearity (Figs. 11b, 11c). Crustal accretion, which began in the area of the stronger block, passed asymmetrically with numerous jumps of the spreading axis, was accompanied by the formation of offsets and a coarse and more dissected topography as compared to neighboring segments (Figs. 11c, 11d). Displacements in the process of accretion of the new model crust transferred to transpressive faults and then to strike-slip faults of a transform type (Figs. 11d, 11e).

Hot Spot Influence on the Development of Rift Fracture at the Presence of Transform Offset with Stronger Lithosphere

An abrupt change in axial morphology frequently occurs along the SEIR strike from the axial rise to the rift valley even at neighboring segments separated by a transform fault (Fig. 3a). At a similar spreading rate in these segments, such changes in morphology can be associated only with the presence of local temperature variations in the mantle. To explain this in the third series, an experiment was performed in which two segments were separated by the cross structure with stronger lithosphere and the local heat source functioned in one segment, forming a thermal anomaly above it in the model asthenosphere (Fig. 8c).

Experiment 5 no. 697 (Fig. 12)

According to the methodology described in [32], a linear thinned zone simulating the heated rift zone with a width of $w = 2$ cm (~20 km in nature) was set in the model lithosphere. It was complicated by offset with a length of $x = 4$ cm. Thickness H_3 of the model lithosphere in the offset zone was two times higher than H_2 in rift segments but lower than thickness H_1 of the model plate. The LHS was switched on at the moment the model began to cool (preparation of the initial model plate), i.e., prior to its stretching. It was located below the offset under the weakened (rift) zone with the reduced thickness of the brittle layer. Due to the relatively low stretching rate, a system of segmented fractures appeared ~30 s after stretching began in the upper segment. It moved in the direction of the inner corner of the offset. In turn, the fracture from the area of the inner corner started developing through the offset zone. They united very quickly into one fracture, and it reached the boundary of the weakened offset zone and the model plate. The fracture that developed from the lower segment formed later and entered the offset zone after the fracture of the upper

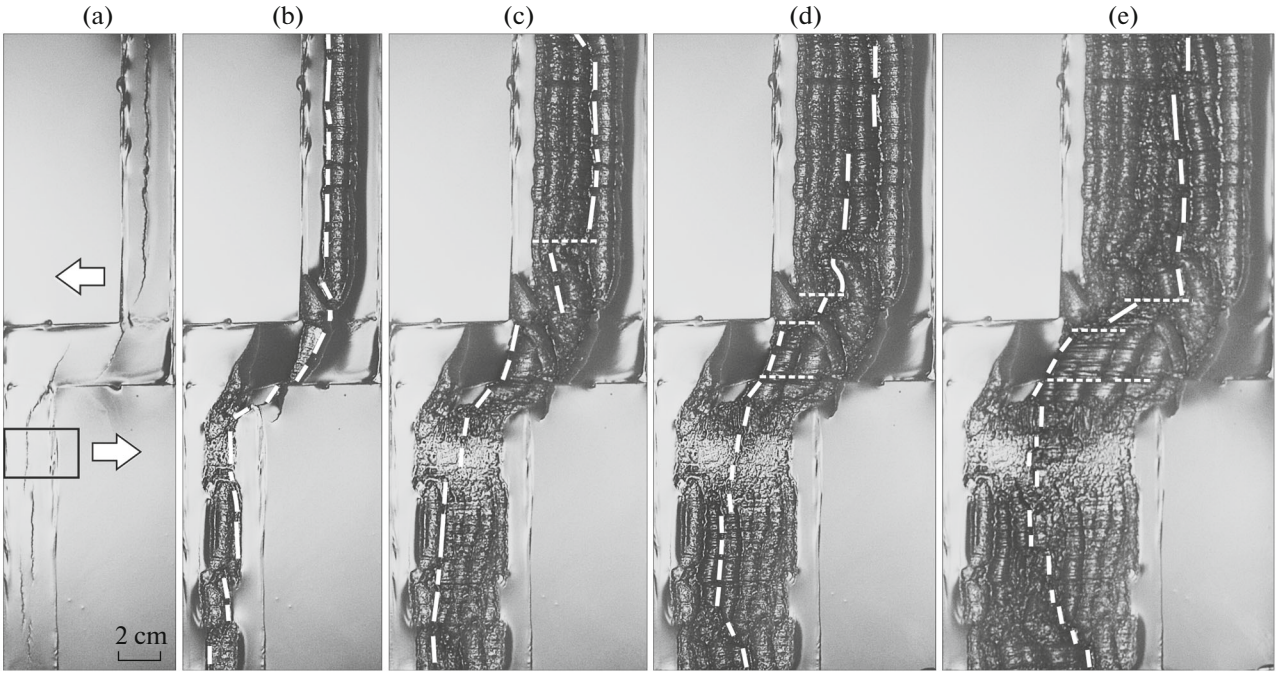

Fig. 12. Experiment 5 no. 697. Evolution of topography in model with hot spot and with inhomogeneity in form of offset with increased thickness. $V = 1.67 \times 10^{-5}$ m/s; $H_1 = 5 \times 10^{-3}$ m; $H_2 = 2 \times 10^{-3}$ m; $H_3 = 1 \times 10^{-3}$ m; $w = 4 \times 10^{-3}$ m; $L_{\text{rift–LHS}} = 0$; $t_{\text{LHS}} = 0$; $\underline{U}_{\text{LHS}} = 200$ v. (a)–(e) Experimental stages. Photograph, plan view For legend, see Fig. 9.

segment (Fig. 12a). Then, the fracture of the upper segment developed through the inner corner of the lower segment and became related to its fracture. Meanwhile, it separated the thickest part of the model lithosphere contacting the weakened zone in the area of the inner corner of the lower segment (Fig. 12b). The topography of the newly formed model crust was formed during extension at the model surface, similar to the previous experimental series. In this experiment, the axis of accretion in the segments was more linear and stable than at the experiments of the previous series due to the effect of not only the LHS but also the general stabilizing effect of the weakened zone. In the offset zone, the oblique strike of the forming morphostructures was inherited from the initial obliquity of the developing fractures. The amplitude of the topography here was higher than in rift segments and significantly higher than in the influence zone of the thermal anomaly (Figs. 12d, 12e). Shallower topography than usual was observed in the area above the LHS, because it was switched on early (Figs. 12b–12d). After the model reached the stationary regime of accretion (V_{spr}, cooling and LHS work ratio), the amplitude of topography increased here (Fig. 12e). At the beginning of the experiment, the spreading axis was located above the left margin of the LHS (Fig. 12a), but as the model crust asymmetrically accreted, it migrated and at later stages it was pulled towards its right boundary (Fig. 12e).

Therefore, the experimental modelling showed that the presence of thermal anomalies in the mantle near the spreading ridge significantly influences the nature of crustal accretion and the formation of axial and off-axial structures. Moreover, the presence of a hot spot in the structure of the sublithosphere mantle will significantly influence the geometry of the rift axis and its position in relation to the hot spot. The hot spot "pulls" the rift axis, the location of which is stabilized above it. In this case, an area of anomalously heated topography is formed on the axis and in its surroundings, and morphological traces of the hot spot influence, similar to the ASP hot spot, remain in the off-axis flank zones. In zones of the relatively cold mantle, a more contrasting and dissected topography is formed during crustal accretion. The spreading axis becomes less linear and is frequently disturbed by nontransform and transform offsets during its evolution.

CONCLUSIONS

Analysis of the peculiarities of topography changes of the SEIR rift zone spreading with an intermediate spreading rate showed that the transit type of morphology is typical of it in general. The main peculiarity of the transit morphology is the change in the topography of the rift zone from axial rises, which resemble the axial rises of the East Pacific Rise, to rift valleys, the topography of which is similar to the topography of MAR rift valleys. Change in the morphology of the rift zone is also accompanied by a change in morphostructural segmentation, the specifics of magmatism, and the deep structure. Several provinces are identi-

fied along the strike of the SEIR rift zone, either with the typical morphology of the rift valley or with the morphology of the axial rise, which in conditions of a poorly variable spreading rate testifies to the existance of other factors influencing the axial morphology. Provinces with the morphology of axial rises were commonly noted in areas with increased mantle temperature subject to the influence of the ASP hot spot located near the axial zone of the SEIR axis. The Kerguelen mantle plume located at a significant distance from the SEIR axis also influences the temperature regime of the SEIR axial zone, although not as obviously as the ASP, which leads to the formation of the axial rise morphology in the axial zone of the central province.

Analysis of the morphology and morphometry of the rift zone topography showed that a change in the main parameters testifies to the decrease of magmatism in the eastern direction on a regional level. In the province with axial rises in the crust (segments K, L, O, P), according to the morphometric indicators similar to quickly spreading ridges, the probability of the presence of AMCs is extremely high. At the intersegment level, in segments R and S with the transient morphology, changes in the morphometric indicators are irregular, which can be associated with the disappearance and occurrence of an AMC at distinct parts of segments where axial rises are observed. The province of the rift valley and the AAD area are characterized by minimum magmatic activity and the absence of AMCs.

Additional confirmation of the reduction in magmatic activity in the eastern direction are gravity anomalies and the Na8 indicator increasing in this direction, as well as the thickness of the crust decreasing in this direction and estimates of the mantle temperature based on these features of the deep structure of the ridge.

Numerical modelling results showed that at the spreading rates of 6–8 cm/yr, significant changes in the deep structure of the rift zone occur, expressed in the extremely unstable condition of the axial crustal magmatic chamber. It turned out that at similar spreading rates, the mantle temperature is a significant factor that influences the existence of axial magmatic chambers in the crust as well as their shapes and sizes. Depending on the mantle heating (proximity of the hot spot), the sizes of chambers can increase, decrease, or chamber can disappear completely. As the estimates show, a stationary crustal magmatic chamber exists in the crust at intermediate spreading rates of 6–7 cm/yr typical of the SEIR and average mantle temperature values (T_m = 1250°C). When the mantle temperature increases (near hot spots), the crustal chamber becomes larger and gains a higher degree of saturation with the melt, while with a reduction in mantle temperatures far from hot spots, the crustal magmatic chamber gradually decreases until it disappears completely. Such variations in SEIR magmatic structures will significantly influence the nature of crustal accretion and determine the type of axial morphology. In addition to an increase in mantle temperatures in the zone of influence of hot spots, the effective strength of the axial lithosphere changes as well. The seabed topography in these zones becomes less dissected. In the area of the AAD with a colder and stronger lithosphere, the absence of a crustal magmatic chamber and a reduction in magma supply intensity are assumed, which is reflected in the reduction of the crustal thickness, an increase of lithosphere thickness and strength, and the formation of an intensely dissected topography with an unstable spreading axis geometry. This part of the ridge presumably represents the area of the "counter interaction" along-axis asthenospheric flows located at different levels under the lithosphere. The interaction of these flows in the AAD area with a stronger and thicker lithosphere underlain by a relatively cold mantle leads to characteristic deformation of the brittle layer of the lithosphere.

Experimental modelling showed that the presence of a hot spot in the structure of the sublithospheric mantle will influence the geometry of the rift axis and its position in relation to the hot spot. The hot spot can "pull" the rift axis. In this case, an area of anomalously heated topography is formed on the axis and in its surroundings, and traces of low-amplitude topography similar to the ASP hot spot remain in the off-axis flank zones. In zones with a relatively cold mantle with a stronger lithosphere, the nature of its failure and the morphology of the topography will be different. A more contrasting and dissected topography forms during crustal accretion. The spreading axis becomes less linear and is frequently offset by nontransform and transform offsets in the process of its evolution.

Therefore, significant changes in the axial morphology, the character of morphostructural segmentation, peculiarities of magmatism, and the deep structure along the SEIR strike with insignificant variations in the spreading rate are caused by significant variations in the mantle temperature associated with the influence of hot and cold spots.

ACKNOWLEDGMENTS

The work was supported by the Russian Science Foundation (grant no. 16-17-10139).

We thank A.N. Filaretova for her assistance in formatting the manuscript. We also thank the esteemed reviewers, whose constructive comments helped to improve the paper.

REFERENCES

1. A. F. Grachev, "Identification of mantle plumes based on studying the composition of volcanic rocks and their isotopic-geochemical characteristics," Petrology **11**, 562–596 (2003).

2. E. P. Dubinin and S. A. Ushakov, *Oceanic Riftogenesis* (GEOS, Moscow, 2001) [in Russian].
3. E. P. Dubinin, Yu. I. Galushkin, and N. M. Sushchevskaya, "Spreading ridges and transform faults," in *World Ocean*, Vol. 1: *Geology and Tectonics of Ocean. Catastrophic Phenomena in Ocean*, Ed. by L. I. Lobkovskii (Nauchn. Mir, Moscow, 2013), pp. 92–170.
4. N. L. Dobretsov, A. G. Kirdyashkin, and A. A. Kirdyashkin, *Deep Geodynamics* (GEO, Novosibirsk, 2001) [in Russian].
5. L. I. Lobkovskii, A. M. Nikishin, and V. E. Khain, *Contemporary Problems of Geotectonics and Geodynamics* (Nauchn. Mir, Moscow, 2004) [in Russian].
6. V. N. Puchkov, "The controversy over plumes: Who is actually right?," Geotectonics **43**, 1–17 (2009).
7. N. M. Sushchevskaya, L. V. Dmitriev, and A. V. Sobolev, "Petrochemical criterion for classification of hardening glasses of oceanic tholeiites," Dokl. Akad. Nauk SSSR **268**, 953–961 (1983).
8. N. M. Sushchevskaya, T. I. Tsekhonya, E. P. Dubinin, E. G. Mirlin, and N. N. Kononkova, "Formation of oceanic crust in mid-ocean ridges of the Indian Ocean," Geochem. Int. **34**, 963–975 (1996).
9. N. M. Sushchevskaya, Ye. V. Koptev-Dvornikov, N. A. Migdisova, D. M. Khvorov, A. A. Peyve, S. G. Skolotnev, B. V. Belyatskiy, and V. S. Kamenetskiy, "Features of the processes of crystallization and tholeiite magmas of the western end of African-Antarctic Ridge (Shpiss Ridge) in the area of Bouve triple junction," Ross. Zh. Nauk. Zemle **1**, 221–250 (1999).
10. A. I. Shemenda, "Similarity criteria when mechanical simulation of tectonic processes," Geol. Geofiz., No. 10, 10–19 (1983).
11. P. Ball, G. Eagles, C. Ebinger, K. McClay, and J. Totterdel, "The spatial and temporal evolution of strain during the separation of Australia and Antarctica," Geochem. Geophys. Geosyst. **14** (8), 2771–2799 (2013). doi 10.1002/ggge.20160
12. J. M. Baran, J. R. Cochran, S. M. Carbotte, and M. R. Nedimović, "Variations in upper crustal structure due to variable mantle temperature along the Southeast Indian Ridge," Geochem. Geophys. Geosyst. **6** (11), Pap. No. Q11002 (2005). doi 10.1029/2005GC000943
13. J. M. Baran, J. R. Cochran, R. C. Holmes, et al., "Constraints on the mantle temperature gradient along the Southeast Indian Ridge from crustal structure and isostasy implications for the transition from an axial high to an axial valley," Geophys. J. Int. **179**, 144–153 (2009). doi 10.1111/j.1365-246X.2009.04300.x
14. G. Bassi and J. Bonnin, "Rheological modeling and deformation instability of lithosphere under extension – II. Depth-dependent rheology," Geophys. J. **94**, 559–565 (1988).
15. F. Benard, J. Callot, R. Vially, J. Schmitz, W. Roest, and M. Patriat, "The Kerguelen plateau: Records from long-living/composite microcontinent," Mar. Pet. Geol. **27**, 633–649 (2010).
16. S. E. Bryan and R. E. Ernst, "Revised definition of Large Igneous Provinces (LIPs)," Earth Sci. Rev. **86**, 175–202 (2008).
17. J. R. Cochran and J.-C. Sempéré, "The Southeast Indian Ridge between 88°E and 118°E: Gravity anomalies and crustal accretion at intermediate spreading rates," J. Geophys. Res.: Solid Earth **102**, 15463–15487 (1997).
18. M. F. Coffin and O. Eldholm, "Large Igneous Provinces: crustal structure, dimensions, and external consequences," Rev. Geophys. **32**, 1–36 (1994).
19. J. A. Conder, D. S. Scheirer, and D. W. Forsyth, "Seafloor spreading of the Amsterdam–St. Paul hotspot plateau," J. Geophys. Res.: Solid Earth **105**, 8263–8277 (2000).
20. V. Courtillot, A. Davaille, J. Besse, and J. Stock, "Three distinct types of hotspots in the Earth's mantle," Earth Planet. Sci. Lett. **205**, 295–308 (2003).
21. C. Dalton, C. Langmuir, and A. Gale, "Geophysical and geochemical evidence for deep temperature variations beneath mid-ocean ridges," Science **344**, 80–83 (2014).
22. C. DeMets, R. Gordon, and D. Argus, "Geologically current plate motions," Geophys. J. Int. **181**, 1–80 (2010).
23. R. S. Detrick, P. Buhl, E. Vera, J. Mutter, J. Orcutt, J. Madsen, and T. Brocher, "Multichannel seismic imaging of an axial magma chamber along the East Pacific Rise between 9° N and 13° N," Nature **326**, 35–41 (1987).
24. E. P. Dubinin, A. V. Rozova, and A. A. Sveshnikov, "Endogenic nature of variations in the bottom topography of the mid-ocean rift zones with intermediate spreading rate," Oceanology **49**, 265–280 (2009). doi 10.1134/S0001437009020118
25. E. P. Dubinin, A. L. Grokhol'skii, A. V. Kokhan, and A. A. Sveshnikov, "Thermal and rheological state of the lithosphere and specific features of structuring in the rift zone of the Reykjanes Ridge (from the results of numerical and experimental modeling)," Izv., Phys. Solid Earth **47**, 586–599 (2011). doi 10.1134/S0001437009020118
26. E. P. Dubinin, A. V. Kokhan, and N. M. Sushchevskaya, "Tectonics and magmatism of ultraslow spreading ridges," Geotectonics **47**, 131–155 (2013). doi 10.1134/S0016852113030023
27. J. Dyment, J. Lin, and E. T. Baker, "Ridge-hotspot interactions," Oceanography **20**, 102–116 (2007).
28. J. Escartin, G. Hirth, and B. Evans, "Effects of serpentinization on the lithospheric strength and the style of normal faulting at slow-spreading ridges," Earth Planet. Sci. Lett. **151**, 181–189 (1997).
29. Yu. I. Galushkin, E. P. Dubinin, and A. A. Sveshnikov, "A nonstationary model of the thermal regime of axial zones of mid-ocean ridges: Formation of crustal and mantle magma chambers," Izv., Phys. Solid Earth **43**, 130–147 (2007). doi 10.1134/S1069351307020048
30. Yu. I. Galushkin, E. P. Dubinin, and A. A. Sveshnikov, "Rheological layering of the oceanic lithosphere in rift zones of the Mid-Oceanic Ridges," Dokl. Earth Sci. **418**, 114–118 (2008). doi 10.1134/S1028334X0801025X
31. GEBCO_08 grid. ver. 20090202. http://www.gebco.net.
32. A. L. Grokholskii and E. P. Dubinin, "Experimental Modeling of Structure-Forming Deformations in Rift Zones of Mid-Ocean Ridges," Geotectonics **40**, 64–80 (2006). doi 10.1134/S0016852106010067
33. J. Goff, Y. Ma, A. Shah, J. Cochran, and J.-C. Sempéré, "Stochastic analysis of seafloor morphology on the flank of the Southeast Indian Ridge: The influence of ridge morphology on the formation of abyssal hills," J. Geophys. Res.: Solid Earth **102**, 15521–15534 (1997).
34. D. Graham, K. Johnson, L. Douglas Priebe, and J. Lupton, "Hotspot–ridge interaction along the

Southeast Indian Ridge near Amsterdam and St. Paul islands: Helium isotope evidence," Earth Planet. Sci. Lett. **167**, 297–310 (1999).

35. D. W. Graham, B. B. Hanan, C. Hemond, J. Blichert-Toft, and F. Albarède, "Helium isotopic textures in Earth's upper mantle," Geochem. Geophys. Geosyst. **15** (5), 2048–2074 (2014). doi 10.1002/2014GC005264
36. R. C. Holmes, M. Tolstoy, J. R. Cochran, and J. S. Floyd, "Crustal thickness variations along the Southeast Indian Ridge (100°–116°E) from 2-D body wave tomography," Geochem. Geophys. Geosyst. **9** (12), Pap. No. Q12020 (2008). doi 10.1029/2008GC002152
37. R. C. Holmes, M. Tolstoy, A. J. Harding, J. A. Orcutt, and J. P. Morgan, "Australian Antarctic Discordance as a simple mantle boundary," Geophys. Res. Lett. **37** (9), Pap. No. L09309 (2010). doi 10.1029/2010GL042621
38. C. Kincaid, G. Ito, and C. Gable, "Laboratory investigation of the interaction of off-axis mantle plumes and spreading centers," Nature **376**, 758–761 (1995).
39. S. H. Kirby, "Rheology of the lithosphere," Rev. Geophys. Space Phys. **21**, 1458–1487 (1983).
40. M. Klein, C. Langmuir, and H. Staudigel, "Geochemistry of basalts from the Southeast Indian Ridge, 115°E–138°E," J. Geophys. Res., [Solid Earth Planets] **96**, 2089–2107 (1991).
41. E. M. Klein and C. H. Langmuir, "Global correlations of ocean ridge basalt chemistry with axial depth and crustal thickness," J. Geophys. Res., [Solid Earth Planets] **92**, 8089–8115 (1987).
42. P. Lonsdale, "Geomorphology and structural segmentation of the crest of the southern (Pacific-Antarctic) East Pacific Rise," J. Geophys. Res.: Solid Earth **99**, 4683–4702 (1994).
43. Y. Ma and J. R. Cochran, "Transitions in axial morphology along the Southeast Indian Ridge," J. Geophys. Res.: Solid Earth **101**, 15849–15866 (1996).
44. K. C. Macdonald, "Linkages between faulting, volcanism, hydrothermal activity and segmentation on fast spreading centers," in *Faulting and Magmatism at Mid-ocean Ridges*, Vol. 106 of *Geophysical Monograph Series*, Ed. by W. R. Buck, P. T. Delaney, J. A. Karson, Y. Lagabrielle (Am. Geophys. Union, Washington, DC, 1998), pp. 27–58.
45. J. Mahoney, D. Graham, D. Christie, K. Johnson, L. Hall, and D. Vonderhaar, "Between a hotspot and a cold spot: Isotopic variation in the Southeast Indian ridge asthenosphere, 86°–118°E," J. Petrol. **43**, 155–1176 (2002).
46. M. Maia, I. Pessanha, E. Sourreges, M. Patriat, P. Gente, C. Hémond, M. Janin, K. Johnson, W. Roest, J.-Y. Royer, and J. Vatteville, "Building of the Amsterdam–Saint-Paul plateau: A 10 Myr history of a ridge – hot spot interaction and variations in the strength of the hot spot source," J. Geophys. Res.: Solid Earth **116** (B9), Pap. No. B09104 (2011). doi 10.1029/2010JB007768
47. B. V. Malkin and A. I. Shemenda, "Mechanism of rifting: Consideration based on results of physical modeling and on geological and geophysical data," Tectonophysics **199**, 193–210 (1991).
48. K. M. Marks, P. R. Vogt, and S. A. Hall, "Residual depth anomalies and the origin of the Australian–Antarctic Discordance zone," J. Geophys. Res., [Solid Earth Planets] **95**, 17325–17337 (1990).
49. K. M. Marks, D. T. Sandwell, P. R. Vogt, and S. A. Hall, "Mantle downwelling beneath the Australian-Antarctic discordance zone: Evidence from geoid height versus topography," Earth Planet. Sci. Lett. **103**, 325–338 (1991).
50. W. J. Morgan, "Rodriguez, Darwin, Amsterdam, ..., a second type of hotspot island," J. Geophys. Res., B **83**, 5355–5360 (1978).
51. K. Okino, K. Matsuda, D. M. Christie, Y. Nogi, and K. Koizumi, "Development of oceanic detachment and asymmetric spreading at the Australian-Antarctic Discordance," Geochem. Geophys. Geosyst. **5** (12), Pap. No. Q12012 (2004). doi 10.1029/ 2004GC000793
52. J.-Y. Royer and R. Schlich, "Southeast Indian ridge between the Rodriguez triple junction and the Amsterdam and Saint-Paul Islands: Detailed kinematics for the past 20 m.y.," J. Geophys. Res., [Solid Earth Planets] **93**, 13524–13550 (1988).
53. W. B. F. Ryan, S. M. Carbotte, J. O. Coplan, S. O'Hara, A. Melkonian, R. Arko, R. A. Weissel, V. Ferrini, A. Goodwillie, F. Nitsche, J. Bonczkowski, and R. Zemsky, "Global Multi-Resolution Topography synthesis," Geochem. Geophys. Geosyst. **10** (3), Pap. No. Q03014 (2009). doi 10.1029/2008GC002332
54. D. Sandwell, D. Muller, W. Smith, E. Garcia, and R. Francis, "New global marine gravity model from CryoSat-2 and Jason-1 reveals buried tectonic structure," Science **346**, 65–67 (2014).
55. D. S. Scheirer, D. W. Forsyth, J. A. Conder, M. A. Eberle, S.-H. Hung, K. T. M. Johnson, and D. W. Graham, "Anomalous seafloor spreading of the Southeast Indian Ridge near the Amsterdam–St.-Paul Plateau," J. Geophys. Res.: Solid Earth **105**, 8243–8262 (2000).
56. J. G. Schilling, "Fluxes and excess temperatures of mantle plumes inferred from their interaction with migrating mid-ocean ridges," Nature **352**, 397–403 (1991).
57. R. C. Searle, J. A. Keeton, R. B. Owens, R. S. White, R. Mecklenburgh, B. Parsons, and S. M. Lee, "The Reykjanes Ridge: Structure and tectonics of a hot-spot-influenced, slow-spreading ridge, from multibeam bathymetry, gravity and magnetic investigations," Earth Planet. Sci. Lett. **160**, 463–478 (1998).
58. J.-C. Sempéré and J. R. Cochran, "The Southeast Indian Ridge between 88°E and 118°E: Variations in crustal accretion at constant spreading rate," J. Geophys. Res.: Solid Earth **102**, 15489–15505 (1997).
59. A. Shah and J.-C. Sempéré, "Morphology of the transition from an axial high to a rift valley at the Southeast Indian Ridge and the relation to variations in mantle temperature," J. Geophys. Res.: Solid Earth **103**, 5203–5223 (1998).
60. A. I. Shemenda and A. L. Groholsky, "Physical modeling of slow seafloor spreading," J. Geophys. Res.: Solid Earth **99**, 9137–9153 (1994).
61. A. Tikku and S. Cande, "The oldest magnetic anomalies in the Australian-Antarctic Basin: Are they isochrons?," J. Geophys. Res.: Solid Earth **104**, 661–667 (1999).
62. M. Tolstoy, A. J. Harding, and J. A. Orcutt, "Crustal thickness on the Mid-Atlantic Ridge: Bull's eye gravity anomalies and focused accretion," Science **262**, 726–729 (1993).

Translated by S. Bondina